
Defense Special Weapons Agency
Alexandria, VA 22310-3398


DNA-TR-96-16

# Computational Modeling of Underground Tunnels in Intact and Jointed Rock

Yvonne D. Murray
APTEK, Inc.
1257 Lake Plaza Drive
Colorado Springs, CO 80906-3578

January 1997



Technical Report

CONTRACT No. DNA 001-91-C-0140

# DISCLAIMER NOTICE

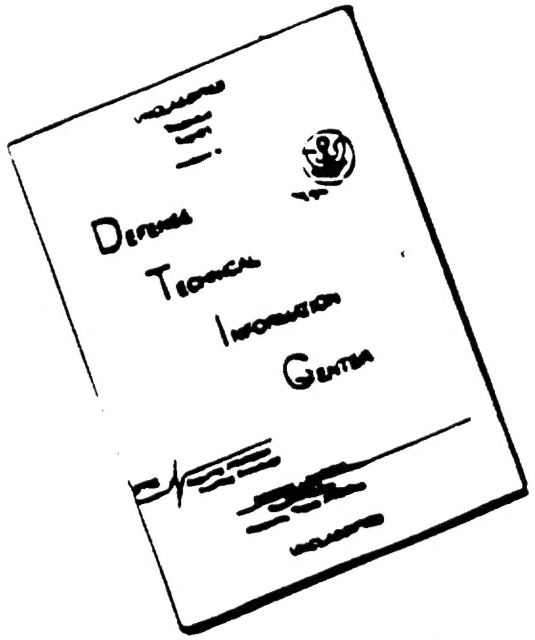

THIS DOCUMENT IS BEST QUALITY AVAILABLE. THE COPY FURNISHED TO DTIC CONTAINED A SIGNIFICANT NUMBER OF PAGES WHICH DO NOT REPRODUCE LEGIBLY.

DESTRUCTION NOTICE:

Destroy this report when it is no longer needed.
Do not return to sender.

PLEASE NOTIFY THE DEFENSE SPECIAL WEAPONS AGENCY, ATTN: CSTI, 6801TELEGRAPH ROAD, ALEXANDRIA, VA 22310-3398, IF YOUR ADDRESS IS INCORRECT, IF YOU WISH IT DELETED FROM THE DISTRIBUTION LIST, OR IF THE ADDRESSEE IS NO LONGER EMPLOYED BY YOUR ORGANIZATION.

# DISCLAIMER NOTICE

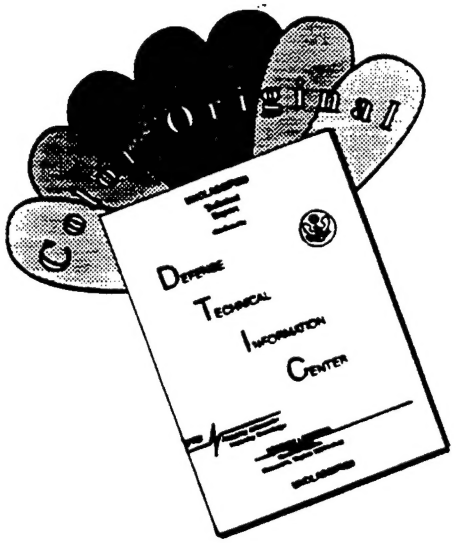


THIS DOCUMENT IS BEST QUALITY AVAILABLE. THE COPY FURNISHED TO DTIC CONTAINED A SIGNIFICANT NUMBER OF COLOR PAGES WHICH DO NOT REPRODUCE LEGIBLY ON BLACK AND WHITE MICROFICHE.

# DISTRIBUTION LIST UPDATE

This mailer is provided to enable DSWA to maintain current distribution lists for reports. (We would appreciate your providing the requested information.)

☐ Add the individual listed to your distribution list.

☐ Delete the cited organization/individual.

☐ Change of address.

**NOTE:**
**Please return the mailing label from the document so that any additions, changes, corrections or deletions can be made easily. For distribution cancellation or more information call DSWA/IMAS (703) 325-1036.**

NAME: _____

ORGANIZATION: _____

| OLD ADDRESS | CURRENT ADDRESS |
|---|---|
| _____ | _____ |
| _____ | _____ |
| _____ | _____ |

TELEPHONE NUMBER: (  ) _____

| DSWA PUBLICATION NUMBER/TITLE | CHANGES/DELETIONS/ADDITIONS, etc.) *(Attach Sheet if more Space is Required)* |
|---|---|
| _____ | _____ |
| _____ | _____ |
| _____ | _____ |

DSWA OR OTHER GOVERNMENT CONTRACT NUMBER: _____

CERTIFICATION OF NEED-TO-KNOW BY GOVERNMENT SPONSOR (if other than DSWA):

SPONSORING ORGANIZATION: _____

CONTRACTING OFFICER OR REPRESENTATIVE: _____

SIGNATURE: _____

CUT HERE AND RETURN

DEFENSE SPECIAL WEAPONS AGENCY
ATTN: IMAS
6801 TELEGRAPH ROAD
ALEXANDRIA, VA 22310-3398

DEFENSE SPECIAL WEAPONS AGENCY
ATTN: IMAS
6801 TELEGRAPH ROAD
ALEXANDRIA, VA 22310-3398

# REPORT DOCUMENTATION PAGE

*Form Approved*
*OMB No. 0704-0188*



| 1. AGENCY USE ONLY (Leave blank) | 2. REPORT DATE | 3. REPORT TYPE AND DATES COVERED |
|---|---|---|
| | 970101 | Technical 910915 - 960315 |

**4. TITLE AND SUBTITLE**
Computational Modeling of Underground Tunnels in Intact and Jointed Rock

**5. FUNDING NUMBERS**
C - 001-91-C-0140
PE - 62715H
PR - RS
TA - RH
WU - DH311560

**6. AUTHOR(S)**
Yvonne D. Murray

**7. PERFORMING ORGANIZATION NAMES(S) and ADDRESS(ES)**
APTEK, Inc.
1257 Lake Plaza Drive
Colorado Springs, CO 80906-3578

**8. PERFORMING ORGANIZATION REPORT NUMBER**
A-96-1R

**9. SPONSORING / MONITORING AGENCY NAME(S) AND ADDRESS(ES)**
Defense Special Weapons Agency
6801 Telegraph Road
Alexandria, VA 22310-3398

PMT/Senseny

**10. SPONSORING / MONITORING AGENCY REPORT NUMBER**
DNA-TR-96-16

**11. SUPPLEMENTARY NOTES**
This work was sponsored by the Defense Nuclear Agency under RDT&E RMC Code B4662D RS RH 00128 4300A AC 25904D.

**12a. DISTRIBUTION / AVAILABILITY STATEMENT**
Approved for public release; distribution is unlimited.

**12b. DISTRIBUTION CODE**

**13. ABSTRACT (Maximum 200 words)**

Computational models were developed to predict the dynamic response and damage to reinforced tunnels in rock subjected to ground shock from nuclear weapons. This effort is part of the Underground Technology Program. The finite element calculations were performed with the DYNA3D code using a comprehensive smooth-cap model for intact rock and a nonlinear slideline model for rock joints. Calculated tunnel closures, and free-field stress and velocity histories, compare well with spherical wave tests (SWAT) on aluminum lined tunnels in intact limestone. The intact rock model includes a scalar anisotropic damage formulation for modeling strain-softening and modulus reduction, viscoplastic formulations and rate-shifted damage surfaces for modeling rate effects, and a three-invariant plasticity formulation. Preliminary ''stack of bricks'' calculations were also performed to verify our joint model, in preparation for future predictions of tunnel response in jointed limestone.

| 14. SUBJECT TERMS | | | 15. NUMBER OF PAGES |
|---|---|---|---|
| Smooth-Cap | Rocks | Joints | 56 |
| Rate Effects | DYNA3D | Closure | 16. PRICE CODE |
| Underground Tunnels | Ground Shock | Finite Elements | |

| 17. SECURITY CLASSIFICATION OF REPORT | 18. SECURITY CLASSIFICATION OF THIS PAGE | 19. SECURITY CLASSIFICATION OF ABSTRACT | 20. LIMITATION OF ABSTRACT |
|---|---|---|---|
| UNCLASSIFIED | UNCLASSIFIED | UNCLASSIFIED | SAR |

SECURITY CLASSIFICATION OF THIS PAGE

CLASSIFIED BY:
N/A Since Unclassfied

DECLASSIFY ON:
N/A Since Unclassified.

# PREFACE

The goal of the work reported here for the Underground Technology Program (UTP)- Three-Dimensional Calculations, is to predict the dynamic response and damage to reinforced tunnels in intact and jointed rock subjected to ground shock from nuclear weapons. The finite element calculations were performed for the Defense Nuclear Agency (DNA) by Ms. Yvonne Murray of APTEK Inc., and consultant Dr. Leonard Schwer of Schwer Engineering and Consulting Services (SE&CS) under contract DNA001-91-C-0140. The APTEK Program Manager was Dr. Eugene Fitzgerald. The DNA technical monitor was Dr. Paul Senseny.

This report is a concise summary of APTEK's effort, with emphasis on the calculations performed by Ms. Murray. These calculations include dynamic tunnel test and stack of brick simulations, with and without modeling rate effects and damage. This report highlights what we learned and provides recommendations for future efforts. More thorough summaries of our intact rock and joint models are documented in an APTEK technical report (Murray and Lindberg, 1996).

Lessons learned from Dr. Schwer's simulations are documented by Thacker, Riha, and Schwer (1995). These calculations include static and preliminary dynamic tunnel test simulations. Emphasis is on rate-dependent and rate-independent simulations, without modeling damage. This document also compares numerical simulations using the Sandler and Rubin (1979) cap model with the smooth-cap model originally developed by Pelesonne (1989) and enhanced by APTEK. Both Ms. Murray's and Dr. Schwer's calculations were performed as part of the Precision Test Modeler's (PTM) benchmarking and validation effort.

In addition to the modeling and simulation effort described in this report, tunnel kill algorithms for the Lethality Analysis of Buried Structures (LABS) software package were developed by consultant Dr. Herbert Lindberg of LCE Software/Engineering. A technical reference which gives details of the closed-form tunnel kill algorithms and their technical justification is currently available through APTEK (Murray and Lindberg, 1996), and will be published as a DNA topical report at a later date.

# CONVERSION TABLE

Conversion factors for U.S. Customary to metric (SI) units of measurement.

| MULTIPLY ⟶ / TO GET ⟵ | ⟶ BY ⟶ / ⟵ BY ⟵ | ⟶ TO GET / ⟵ DIVIDE |
|---|---|---|
| angstrom | 1.000 000 × E -10 | meters (m) |
| atmosphere (normal) | 1.013 25 × E +2 | kilo pascal (kPa) |
| bar | 1.000 000 × E +2 | kilo pascal (kPa) |
| barn | 1.000 000 × E -28 | meter$^2$ (m$^2$) |
| British thermal unit (thermochemical) | 1.054 350 × E +3 | joule (J) |
| calorie (thermochemical) | 4.184 000 | joule (J) |
| cal (thermochemical)/cm$^2$ | 4.184 000 × E -2 | mega joule/m$^2$ (MJ/m$^2$) |
| curie | 3.700 000 × E +1 | giga becquerel (GBq)* |
| degree (angle) | 1.745 329 × E -2 | radian (rad) |
| degree Fahrenheit | $\tau_K = (t°f + 459.67)/1.8$ | degree kelvin (K) |
| electron volt | 1.602 19 × E -19 | joule (J) |
| erg | 1.000 000 × E -7 | joule (J) |
| erg/second | 1.000 000 × E -7 | watt (W) |
| foot | 3.048 000 × E -1 | meter (m) |
| foot-pound-force | 1.355 818 | joule (J) |
| gallon (U.S. liquid) | 3.785 412 × E -3 | meter$^3$ (m$^3$) |
| inch | 2.540 000 × E -2 | meter (m) |
| jerk | 1.000 000 × E +9 | joule (J) |
| joule/kilogram (J/kg) (radiation dose absorbed) | 1.000 000 | Gray (Gy) ** |
| kilotons | 4.183 | terajoules |
| kip (1000 lbf) | 4.448 222 × E +3 | newton (N) |
| kip/inch$^2$ (ksi) | 6.894 757 × E +3 | kilo pascal (kPa) |
| ktap | 1.000 000 × E +2 | newton- second/m$^2$ (N-s/m$^2$) |
| micron | 1.000 000 × E -6 | meter (m) |
| mil | 2.540 000 × E -5 | meter (m) |
| mile (international) | 1.609 344 × E +3 | meter (m) |
| ounce | 2.834 952 × E -2 | kilogram (kg) |
| pound-force (lbf avoirdupois) | 4.448 222 | newton (N) |
| pound-force inch | 1.129 848 × E -1 | newton-meter (N•m) |
| pound-force/inch | 1.751 268 × E +2 | newton/meter (N/m) |
| pound-force/foot$^2$ | 4.788 026 × E -2 | kilo pascal (kPa) |
| pound-force/inch$^2$ (psi) | 6.894 757 | kilo pascal (kPa) |
| pound-mass (lbm avoirdupois) | 4.535 924 × E -1 | kilogram (kg) |
| pound-mass-foot$^2$ (moment of inertia) | 4.214 011 × E -2 | kilogram-meter$^2$ (kg•m$^2$) |
| pound-mass/foot$^3$ | 1.601 846 × E +1 | kilogram/meter$^3$ (kg/m$^3$) |
| rad (radiation dose absorbed) | 1.000 000 × E -2 | Gray (Gy)** |
| roentgen | 2.579 760 × E -4 | coulomb/kilogram (C/kg) |
| shake | 1.000 000 x E -8 | second (s) |
| slug | 1.459 390 x E +1 | kilogram (kg) |
| torr (mm Hg, 0°C) | 1.333 22 × E -1 | kilo pascal (kPa) |

* The becquerel (Bq) is the SI unit of radioactivity; 1 Bq = 1 event/s.

**The Gray (Gy) is the SI unit of absorbed radiation.

TABLE OF CONTENTS


| Section | | Page |
|---|---|---|
| | FIGURES | vi |
| 1 | INTACT ROCK MODEL AND SWAT SIMULATIONS | 1 |
| | 1.1 INTACT ROCK MODEL OVERVIEW | 1 |
| | 1.2 SWAT TEST OVERVIEW | 1 |
| | 1.3 SWAT COMPUTATIONAL SUMMARY | 2 |
| | 1.4 VISCOPLASTIC MODEL BEHAVIOR | 13 |
| | 1.4.1 Single-Parameter Model | 14 |
| | 1.4.2 Strain-Rate Dependent Extension | 17 |
| | 1.4.3 Pressure-Dependent Extension | 21 |
| | 1.4.4 Inertial Effects | 22 |
| 2 | JOINT MODEL AND STACK OF BRICK SIMULATIONS | 23 |
| | 2.1 JOINT MODEL OVERVIEW | 23 |
| | 2.2 JOINT RATE EFFECTS | 23 |
| | 2.3 STACK OF BRICKS COMPUTATIONAL SUMMARY | 26 |
| 3 | SUMMARY AND LESSONS LEARNED | 30 |
| 4 | REFERENCES | 33 |
| Appendix | | |
| A | FITS OF THE INTACT ROCK MODEL TO DATA | A-1 |
| B | ANALYTICAL SOLUTIONS FOR DUVAUT-LION AND PERZYNA MODELS | B-1 |

# FIGURES


| Figure | | Page |
|---|---|---|
| 1-1 | SWAT dynamic test configuration. . . . . | 2 |
| 1-2 | Close-up of the SWAT-2 finite element mesh near the source and tunnels. | 3 |
| 1-3 | Measured SWAT velocity applied to inner cavity in finite element analysis. . . . . | 3 |
| 1-4 | The rate-independent calculation without damage underpredicts the measured crown-invert closures. . . . . | 4 |
| 1-5 | The rate-dependent calculation without damage is in good agreement with the measured velocity and stress histories, but predicts springline opening instead of closing. . . . . | 6 |
| 1-6 | Modeling rate effects near the source, but not near the tunnels provides good agreement with most of the measured velocity, stress, and closure histories. . . . . | 7 |
| 1-7 | The Mie-Gruenisen model predicts the stiffening behavior of geological materials at high stress better than the constant bulk modulus model. . . | 9 |
| 1-8 | Modeling brittle damage provides more late-time springline closure than the calculations without damage. Here we modeled viscoplasticity near the source, but not near the tunnels. . . . . | 11 |
| 1-9 | This unconfined plane strain simulation is intended to represent conditions at the tunnel springline. Note that little softening is calculated by the damage model. . . . . | 12 |
| 1-10 | SWAT cross-section showing post-test damage near the source and tunnels. | 13 |
| 1-11 | High strain rate data for rocks indicating an increase in strength with strain rate (Handin and Friedman, 1976). . . . . | 14 |
| 1-12 | Good fit of the single parameter Duvaut-Lions ($n = 1$) model to Hopkinson bar data for Solenhofen limestone. . . . . | 15 |
| 1-13 | Poor comparison of the single-parameter Duvaut-Lions smooth cap implementation to concrete data ($n = 1$). . . . . | 16 |
| 1-14 | The rate effect increases with confining pressure for Solenhofen limestone data (Hopkinson bar enclosed in a pressure vessel). . . . . | 17 |
| 1-15 | The peak stress attained with the Duvaut-Lions smooth cap implementation appears to lie on a 'shifted' plasticity surface. . . . . | 18 |

FIGURES (Continued)


| Figure | | Page |
|---|---|---|
| 1-16 | The rate effect decreases with confining pressure for the Duvaut-Lions smooth cap implementation. | 19 |
| 1-17 | Good comparisons of the strain-rate dependent viscoplastic model with concrete data ($n = 5$). | 20 |
| 1-18 | The pressure-dependent viscoplastic model fits Salem limestone Hugoniot data better than the pressure-independent model. | 21 |
| 2-1 | The nonlinear joint model fits normal compressibility data better than the linear model. | 24 |
| 2-2 | Joint shear benchmark geometry and loading. | 25 |
| 2-3 | Preliminary joint sliding calculations with and without rate effects ($\beta = 100$ indicates rate effects). | 26 |
| 2-4 | Stack of bricks layup and gage locations. | 27 |
| 2-5 | Modeling irregular gaps produces asymmetric damage patterns in the preliminary "stack of bricks" simulation. An asymmetric damage pattern was also observed in the stack of bricks test. | 28 |
| 2-6 | The preliminary SOB stress-strain history calculated with initial gaps is more nonlinear than that calculated without initial gaps. | 29 |
| A-1 | Good fits of model to triaxial extension data for Salem limestone. | A-2 |
| A-2 | Good fits of model to triaxial compression data for Salem limestone | A-3 |
| A-3 | Uniaxial strain behavior of the model at four strain rates for two different fits to data. | A-4 |
| A-4 | Assumed strength versus strain rate behavior of model showing greater rate effects in tension than in compression. | A-5 |
| A-5 | Uniaxial stress behavior of the model at four strain rates. | A-6 |
| B-1 | Numerically calculated strength enhancement indicating that the $n = 1$ solution has the steepest slope. | B-3 |

# SECTION 1

# INTACT ROCK MODEL AND SWAT SIMULATIONS

## 1.1 INTACT ROCK MODEL OVERVIEW.

Performing calculations with a first principles code requires implementation of a comprehensive material model for rock and other geological materials. We implemented a smooth-cap model with damage into the nonlinear finite element code DYNA3D (Whirley, 1993) to analyze the static and dynamic response of tunnels in intact rock. The original basis of our geological material model is a two-invariant, smooth-cap elasto-plastic model (Pelesonne, 1989). We added numerous features to this model to improve fits to standard laboratory test data. These improvements include a scalar *anisotropic damage* formulation for modeling strain-softening and modulus reduction, *viscoplastic/viscodamage* formulations and *rate-shifted damage thresholds* for modeling high strain rate effects, an *element length scale* to regularize the damage dissipation to be mesh size independent, and a *three-invariant plasticity*[1] formulation to simultaneously fit triaxial tension and compression data. The model captures the essential features of geological material behavior; shear enhanced compaction, dilatency, pre-peak hardening, post-peak softening, modulus reduction, and localized damage accumulation. Good fits of the model to quasi-static and high strain rate data are given in Appendix A.

## 1.2 SWAT TEST OVERVIEW.

SRI conducted spherical wave tests (SWAT) on aluminum lined tunnels in limestone cylinders (Klopp *et. al*, 1995), as shown in Figure 1-1. The objective of these tests was to increase our understanding of dynamic tunnel closure mechanisms and to provide data for model verification. Numerous tunnels were simultaneously tested and located at various distances the center of the PETN charge. SRI recorded free-field velocity and stress histories, and the crown-invert and springline closures.

Using our physically-based model, we calculated tunnel closures, free-field stress histories, and free-field velocity histories for comparison with the recorded SWAT data. Our finite element mesh with two tunnels modeled at 14.5 cm and 19.2 cm is shown in Figure 1-2. Instead of modeling the explosive charge, we applied the measured velocity history shown in Figure 1-3 to the inside of the 7.5 cm radius cavity. This is the velocity recorded by gage PV1 at that location.

SRI measured the closures on the liner, not the tunnel. Hence we report predicted liner closures, rather than tunnel closures. We modeled a frictionless sliding interface between the tunnel and liner which allows the liner to separate from the tunnel. The 0.79-mm thick liner is made of annealed aluminum and modeled as an elastic-plastic material. SRI did not report whether the liner separated from the tunnel during the test.

[1]This formulation was implemented, in part, on DNA's Conventional Weapons Effects Program and is reported by Murray and Lewis (1995) and Schwer and Murray (1994).

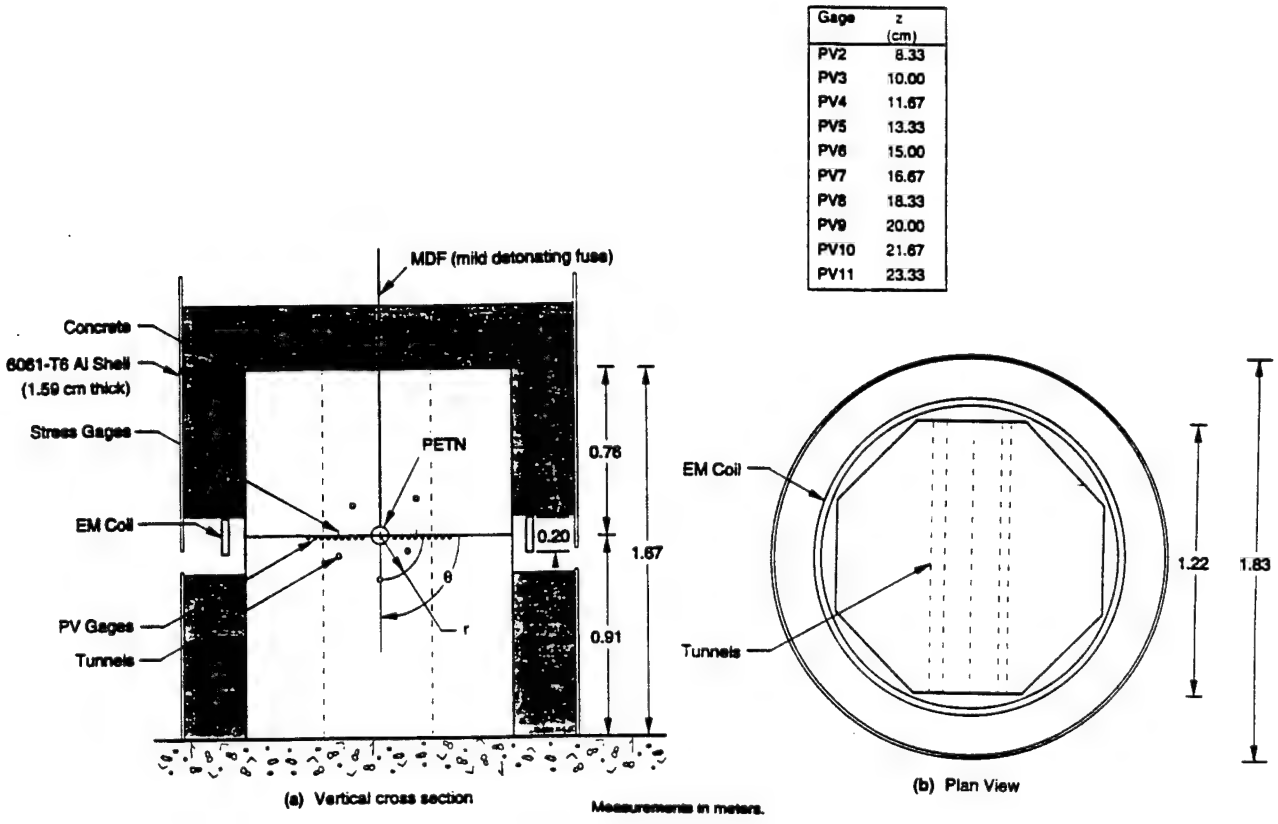


Figure 1-1. SWAT dynamic test configuration.

Numerous calculations were performed and compared with test data to determine the effects of modeling strain-rate dependence and damage. Comparisons include liner closures at the 14.5 cm and 19.2 cm tunnel locations, free field velocity histories at 8.33 cm (PV2), 13.33 cm (PV5), 18.33 cm (PV8), and 23.33 cm (PV11) from the center of the charge, and free field stress histories at 14.5 cm and 19.2 cm.

## 1.3 SWAT COMPUTATIONAL SUMMARY.

Overall, the *rate-independent* calculation without damage simulates the free-field velocity and stress histories reasonably well, although the calculated peak velocities and late-time stress histories are slightly lowered than measured. This is demonstrated in Figure 1-4. However, the calculated crown-invert closure at 14.5 cm is about 25% lower than measured[2]. In addition, the calculated crown-invert closure at 19.2 cm is about 50% lower than measured, and does not exhibit the rebound of the measured closure.

One possible explanation for the difference between the measured and calculated crown invert closures at 19.2 cm is that the liner separated from the tunnel during the test, then

[2]In Figures 1-4a and 1-4b we show both the crown-invert and springline closures on a single plot. Using the tunnel located at 14.5 cm as an example, the calculated crown-invert closure is about 5% while the measured closure is about 6.7%. The calculated springline closure is about 1% while the measured closure is about 2%.

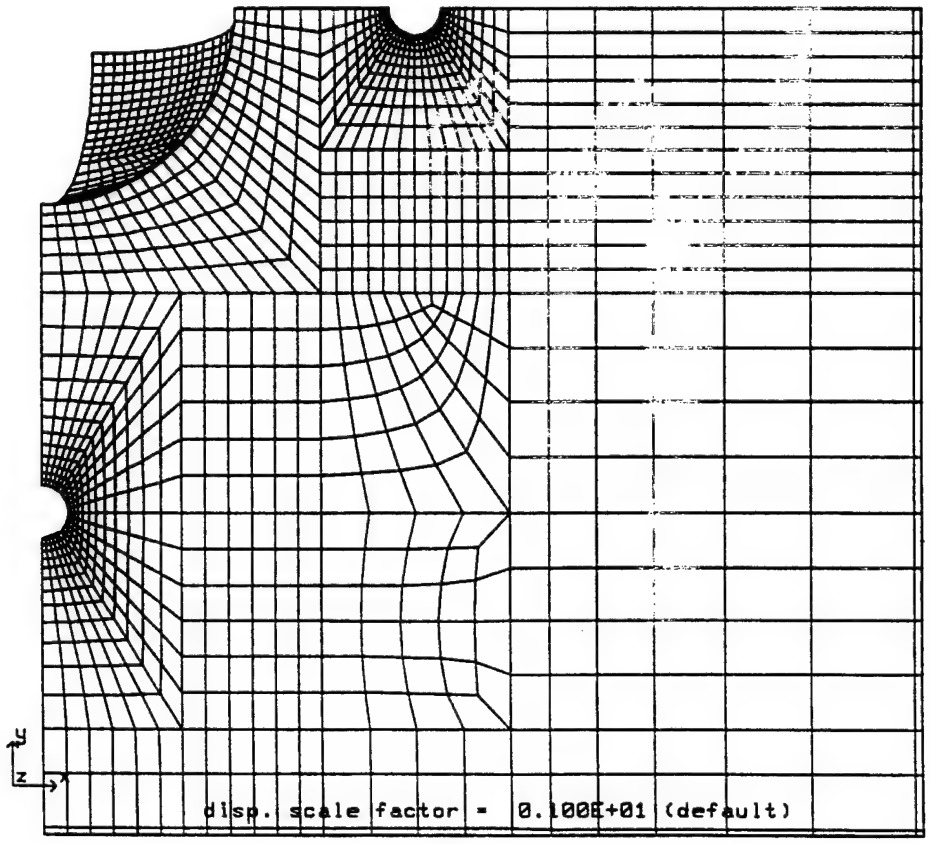


Figure 1-2. Close-up of the SWAT-2 finite element mesh near the source and tunnels.

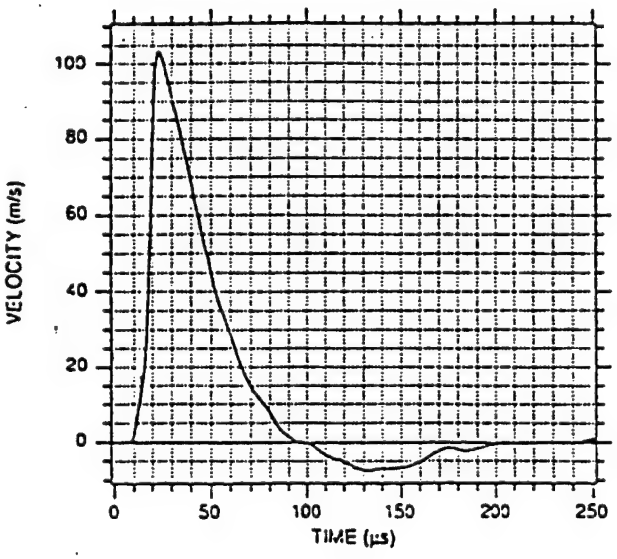


Figure 1-3. Measured SWAT velocity applied to inner cavity in finite element analysis.

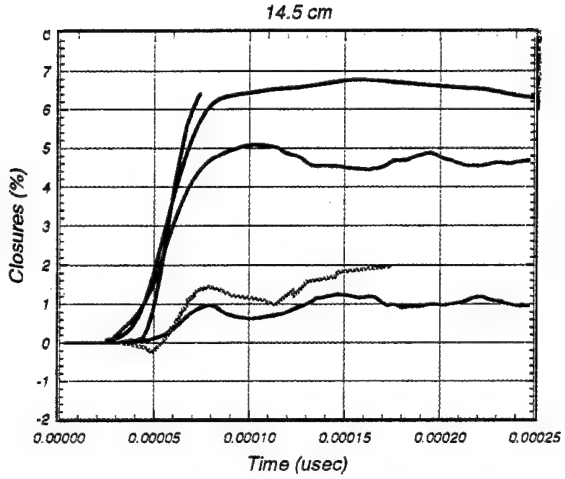


(a) Closures at the 14.5 cm tunnel.

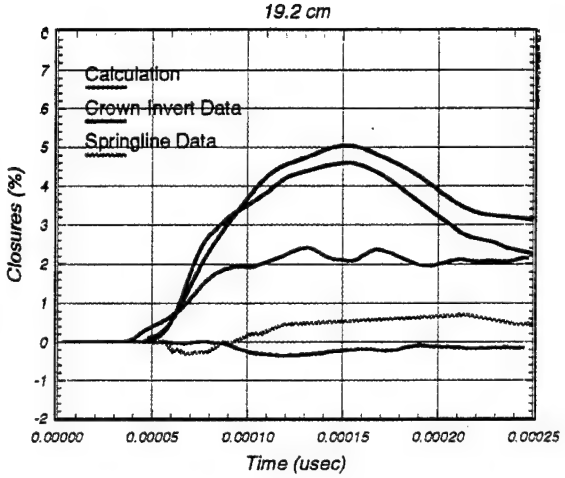


(b) Closures at the 19.2 cm tunnel.

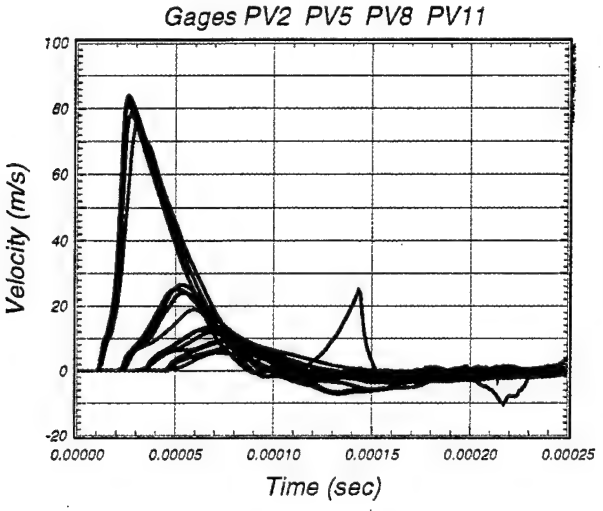


(c) Velocity histories at four gage locations.

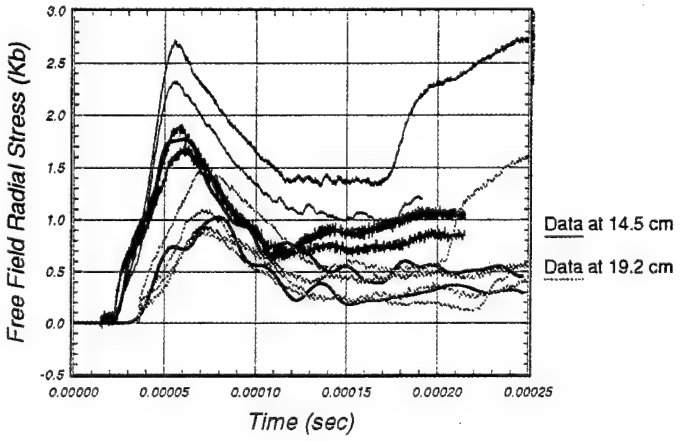


(d) Stress histories at two gage locations.

Figure 1-4. The rate-independent calculation without damage underpredicts the measured crown-invert closures.

rebounded to join the tunnel at late time (around 0.25 msec). The liner did not separate from the tunnel during the calculation, although the calculated tunnel closure is in agreement with one late time measurement. Some preliminary calculations with a less refined mesh indicated separation at this tunnel location.

Adding *viscoplasticity* (rate-dependence) to the calculation without damage improves comparisons between the measured and calculated velocity histories, and between the measured and calculated crown-invert closure at the 14.5 tunnel location. This is demonstrated in Figure 1-5. However, viscoplasticity has little effect on the crown-invert closure calculated at the 19.2 cm tunnel. Modeling viscoplasticity also *opens* the springline closures at both tunnel locations, in lack of agreement with the measured histories. We note that the measured springlines open slightly at early time (around 0.5-0.6 msec) before closing. Our calculation starts out with the right springline opening, but continues to open instead of close. This suggests that some mechanism, not currently modeled, initiates the closing. However, SRI reports that the resolution of the gages is 0.3% of the tunnel closure (Klopp *et. al.*, 1995), and the initial opening/closing is on the order of this resolution.

Modeling *viscoplasticity near the source*, but not near the tunnels, provides excellent agreement between the measured and calculated histories at almost all locations. This is demonstrated in Figure 1-6. One exception is the crown-invert closure at the 19.2 cm tunnel in which the calculated closure agrees with the measured closure at late time, but not throughout the entire history. The other exception is the early-time opening/closing behavior.

It is interesting to note the free-field velocity and stress histories calculated in Figures 1-5 and 1-6 are only subtlety different, yet the calculated springline closures are significantly different (of opposite sign). By not modeling of rate effects near the tunnel, we were able to change the calculated springline deformation from opening to closing at the 14.2 cm location.

To help understand these correlations, it is necessary to examine the implementation of the viscoplastic model and how it was fit to high strain rate data. The behavior of the viscoplastic model and fits to high strain rate data are thoroughly discussed in the Section 1.4, so only the pertinent issues are discussed here.

Effectively, we model different rate effects on the cap than on the shear failure surface. This is done by fitting our viscoplastic model to two sets of data, with a smooth transition between fits. These data are high pressure data (on the cap) and uniaxial stress data (on shear failure surface). Examples of high pressure data are Hugoniot data or SWAT free-field data. We set the cap (pressure-dependent) viscoplastic parameters to get good agreement with the SWAT PV 2 velocity gage history[3]. We *approximately* set the the shear failure surface parameters to fit Hopkinson split pressure bar data (compressive). Based on a general review of Hopkinson bar data available in the literature, including that for Solenhofen limestone (Salem limestone data was not available), we assumed that strength enhancement increases

[3]We also fit the pressure-dependent viscoplastic parameters to Salem Limestone Hugoniot data available in the literature, as discussed in Appendix A. However, the SWAT velocity history correlations, using the Hugoniot fit, were not as good as those shown in Figure 1-5, using the PV2 gage fit, so they are not shown here. Similarly, modeling viscoplasticity near the tunnel (with the Hugoniot fit) *opened* the springline slightly, consistent with the trend already noted.

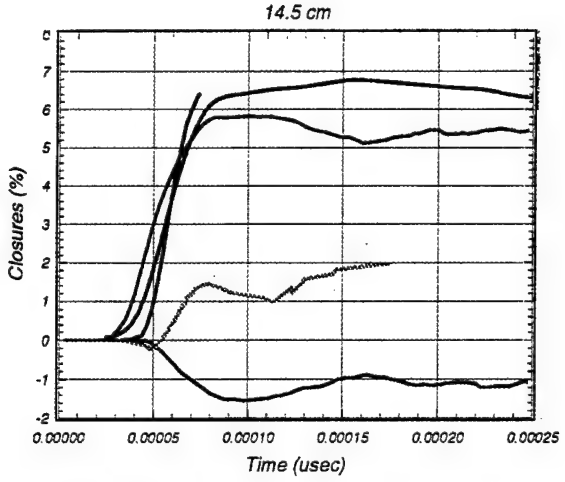


(a) Closures at the 14.5 cm tunnel.

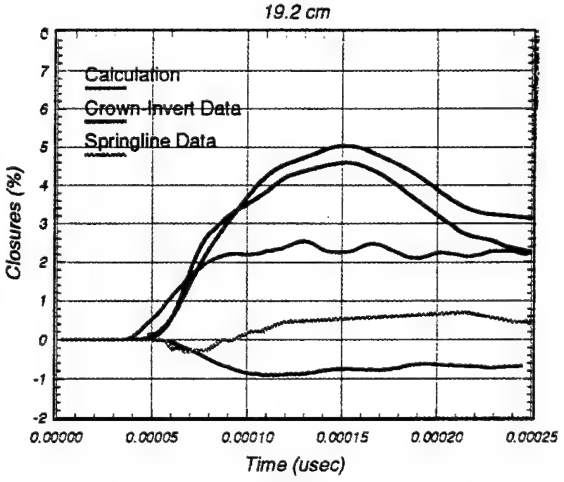


(b) Closures at the 19.2 cm tunnel.

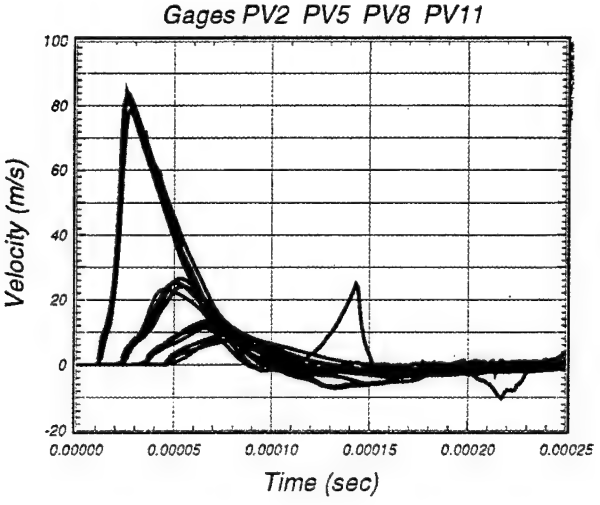


(c) Velocity histories at four gage locations.

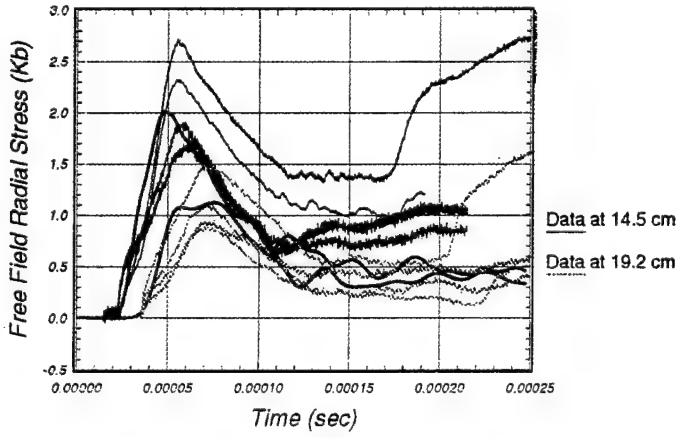


(d) Stress histories at two gage locations.

Figure 1-5. The rate-dependent calculation without damage is in good agreement with the measured velocity and stress histories. but predicts springline opening instead of closing.

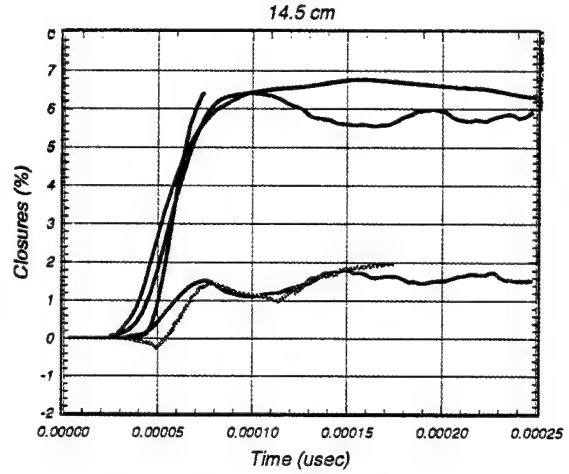


(a) Closures at the 14.5 cm tunnel.

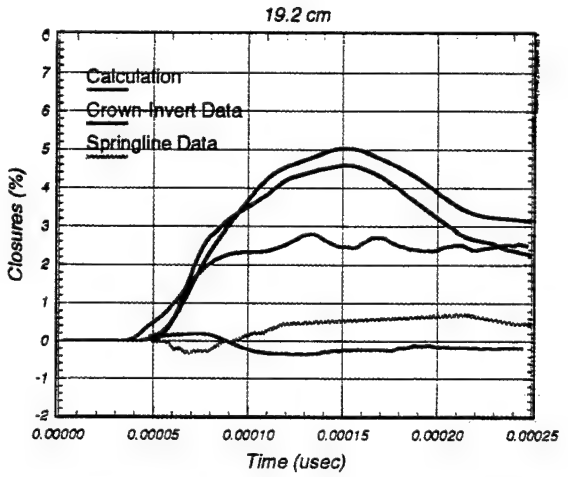


(b) Closures at the 19.2 cm tunnel.

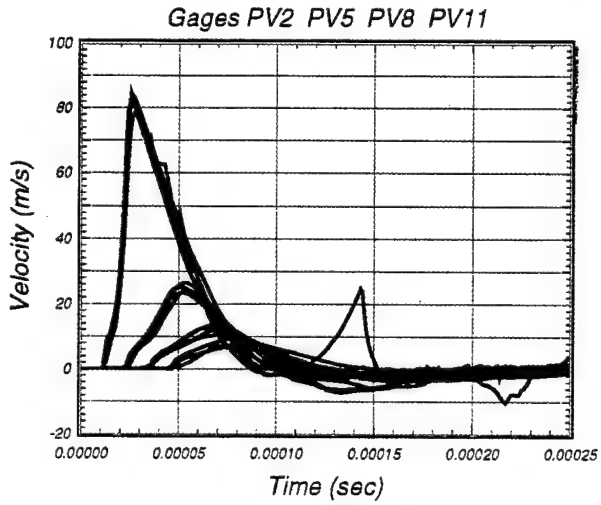


(c) Velocity histories at four gage locations.

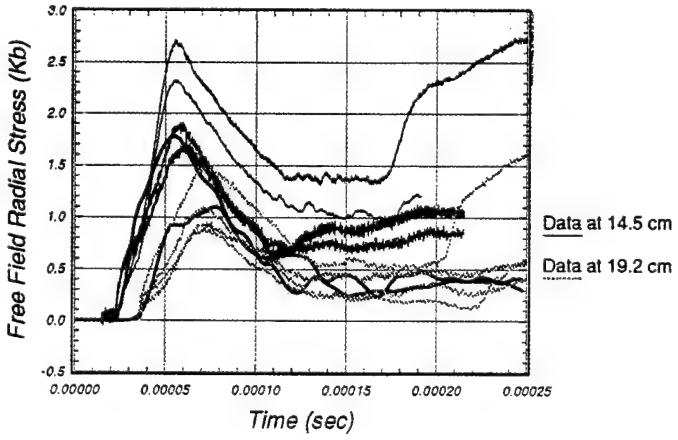


(d) Stress histories at two gage locations.

Figure 1-6. Modeling rate effects near the source, but not near the tunnels provides good agreement with most of the measured velocity, stress, and closure histories.

by a factor of two at high strain rates near $10^4$. Hopkinson bar data for Solenhofen limestone is given in Figure 1-12 of Section 1.4.

The observation that we calculate the free-field velocity and stress histories adequately in Figure 1-5, but not the springline closures, suggests that we model high pressure (cap) rate effects adequately, but not low pressure (shear failure surface) rate effects. Near the source, the pressure is high and the stress state lies on the cap. Near the tunnels, the pressure is low and the stress path encounters the shear failure surface. We attempted one calculation in which we modeled minimal rate effects on the shear failure surface; we assumed that strength enhancement increase by 10% at high strain rates near $10^4$, but this calculation did not improve correlations with the springline measurement. The only way we achieved good correlations with the springline measurement was to turn viscoplasticity off completely near the tunnels, as previously demonstrated in Figure 1-6.

Two alternative, but tentative conclusions could be drawn here. The first conclusion is that our fits[4] and/or viscoplastic formulation need tuning. This conclusion is partly supported by the SWAT correlations of other PTM group calculators, specifically Weidlinger & Associates (WA) and Titan Research Corporation (TRT). By adjusting their rate-dependent fits on the cap, and modeling minimal rate effects on the shear failure surface, both calculators were able to simulate springline closure at the 14.2 cm tunnel. However, at the time this report was written, no PTM calculator was able to simulate the the crown-invert rebound and slight springline closure measured at the 19.2 cm tunnel. In addition, no calculator demonstrated that tuning the viscoplastic model to the SWAT data provides a good predictive capability for other tunnel tests, because no such predictions were made. Future efforts should include additional tunnel response predictions, particularly for full scale field tests.

The second possible conclusion is that we need to examine alternatives to viscoplasticity, such as rate-shifted plasticity surfaces or better dynamic stress-strain relations. When generating high strain rate Hugoniot data like that shown in Figure A-3a of Appendix A, peak stress and strain values are *derived* from measured shock and particle velocity histories (Larson and Anderson, 1979). This derivation is usually based conservation laws for uniaxial flow, or the Rankine-Hugoniot jump equations. Viscoplasticity is not assumed in the derived stress/strain values, although pore collapse rate effects, if any, may affect the measured particle velocity histories.

All PTM calculators, including APTEK, used a constant bulk modulus model for the pressure-volumetric strain relation, as follows:

$$P = K(\epsilon_v - \epsilon_v^p) \tag{1.1}$$

where $P$ is the pressure, $K$ is the bulk modulus, $\epsilon_v$ is the total volumetric strain, and $\epsilon_v^p$ is the plastic volumetric strain. Once all pores are collapsed, $\epsilon_v^p$ remains constant its maximum value, so Equation 1.1 simulates a *linear* relation between the pressure and volumetric strain, at least at high pressure.

[4]One difference between our fits to laboratory data, and those of the other PTM calculators, is that our cap was initially located at a lower pressure than those of the other calculators. This could make a difference when modeling pressure-dependent rate effects.

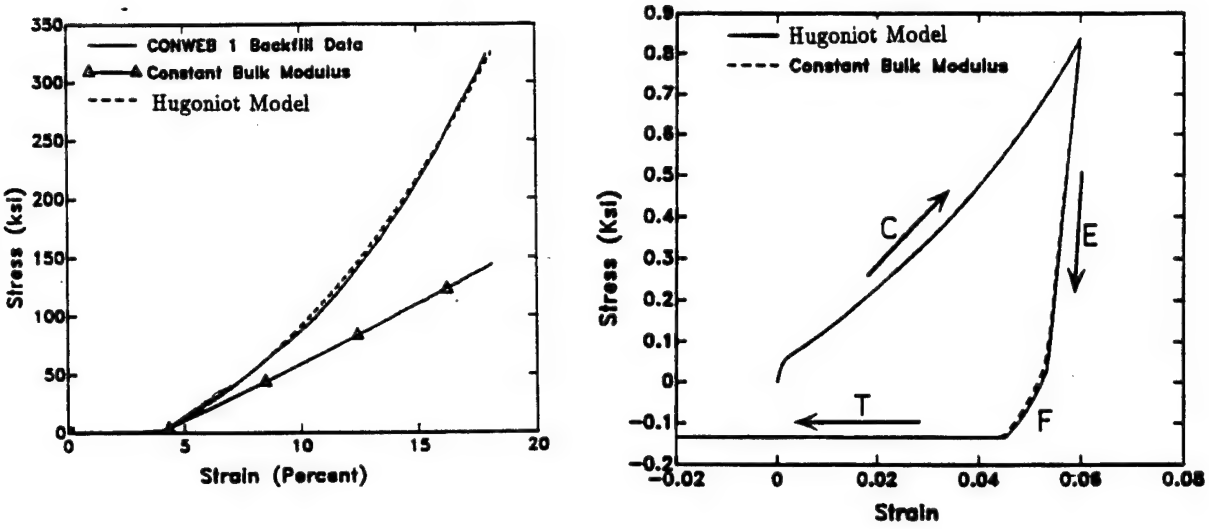


(a) High stress behavior. (b) Low stress behavior.

Figure 1-7. The Mie-Gruenisen model predicts the stiffening behavior of geological materials at high stress better than the constant bulk modulus model.

For consistency in interpreting and fitting Hugoniot data, we suggest evaluating an alternative pressure-volumetric strain relation, based on the Rankine-Hugoniot relations for a travelling shock wave, and the assumption of a linear shock-velocity versus particle velocity relationship, as follows:

$$P = \frac{\rho c^2 \phi_c}{(1 - S\phi_c)^2} \tag{1.2}$$

where $\rho$ is the density, $c$ is the bulk sound speed, $S$ is the slope of the linear fit to the shock velocity versus particle velocity data, and $\phi_c$ is the relative change in volume of the solid particles. $\phi_c$ depends on the total and plastic volume strains, as discussed by Murray and Lewis (1995). This relation was incorporated into an explicit pore collapse model with a Mie-Gruniesen equation of state on DNA's CWE program. The three user-supplied material parameters for the Gruenisen model are $c$ (or $K = \rho c^2$) and $S$ and the Gruenisen parameter $\Gamma$, compared with $K$ for the constant modulus model.

Although the Mie-Gruniesen model was not used on the current UTP program, a fit to soil data was previously made on the CWE program which illustrates the *general behavior* of the model. The low stress behaviors of the constant modulus model in Equation 1.1 and the Mie-Gruniesen model in Equation 1.2 are nearly identical, but the high stress behaviors differ, as shown in Figure 1-7. Equation 1.2 simulates a nonlinear relation between the pressure and volumetric strain, which *stiffens* at high stress levels.

Future efforts should examine the specific behavior of the Mie-Gruniesen and constant bulk modulus models for Salem limestone, using approximate values for $S$ and $\Gamma$ available for limestone (or rock) in the literature. We recommend simulating the Hugoniot velocity records measured by Larson and Anderson, because they are measured histories, not derived quantities like the peak stress values. We want to determine if good correlations with the velocity

records require the use of a rate effects model, and if so, how rate effects should be related to pore collapse. If the rate effects and/or stiffening behavior are significant, then we recommend performing additional SWAT calculations with the Mie-Gruniesen model. The appealing aspect of the Mie-Gruniesen model is that we expect it to simulate higher stress levels near the SWAT source (high pressure regime) than the rate-independent constant bulk modulus model, but not near the tunnels (low pressure regime). This is exactly what we accomplished by modeling viscoplasticity near the source in Figure 1-6, but not near the tunnels.

Adding *brittle damage* to the calculation with viscoplasticity modeled near the source (but not near the tunnels) increases the late-time springline closures, but has little effect on the crown-invert closures or the velocity and stress histories, as shown in Figure 1-8. The effect of brittle damage on the springline closures is most noticeable after about 0.15 msec. The brittle damage model degrads the moduli in the directions of principal *tensile* stress, once an initial energy threshold is exceeded. Our damage model is loosely based on research by Ju (1989). Overall, the calculation is in excellent agreement with the data.

In addition to the damage calculation just discussed, we ran additional brittle damage calculations with and without modeling viscoplasticity near the source and tunnels, but the trends were always similar. Brittle damage either increased, or had little effect, on the late-time springline closures. In some cases, reductions in the late-time stress and velocity histories were calculated (after about 0.10 msec).

Adding *ductile damage* to the brittle damage calculations did not improve comparisons with the measured data, with or without modeling viscoplasticity, so results are not shown here. For example, adding ductile/brittle damage to the viscoplastic calculation previously shown in Figure 1-5 reduces the late-time stress histories, in poor agreement with the measured data, and increases the late-time springline closures. The ductile damage model degrads the moduli in the directions of principal *compressive* stress, once an initial energy threshold is exceeded. This degradation is pressure-dependent, so substantial damage occurs only in the low pressure regime (below about 25 MPa).

The reason we implemented ductile damage in addition to brittle damage is that our brittle damage implementation did not simulate a "cross effect" between degradation in one principal direction and degradation in another, as suggested by Ortiz (1985). This was true even when we attempted to model brittle damage based on tensile strain directions rather than tensile stress directions[5]. An example of modeling the cross effect is an unconfined compression simulation in which damage initiates in the lateral directions (due to the presence of lateral tensile strains), causing the specimen to soften in the axial direction (in the presence of axial compressive strains). We were unable to simulate axial softening with the brittle model, unless ductile damage was also implemented. Efforts are in progress to develop a

[5]When implementing a scalar anisotropic model, one must choose a criteria for damage evolution, and define the projection operators (direction of damage). For example, scalar damage criteria are often based on the history of strains, stress, or energy, while projection operators are based on the directions of maximum principal strain or stress. We implemented an energy-based damage model and separately examined the use of projection operators based on maximum principal stress and maximum principal strain. However, neither implementation simulated a "cross effect."

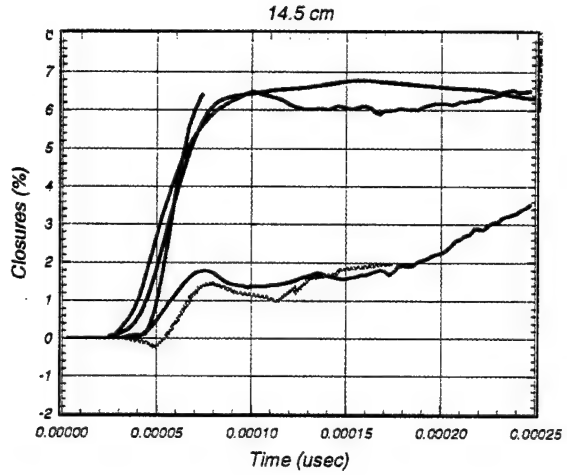


(a) Closures at the 14.5 cm tunnel.

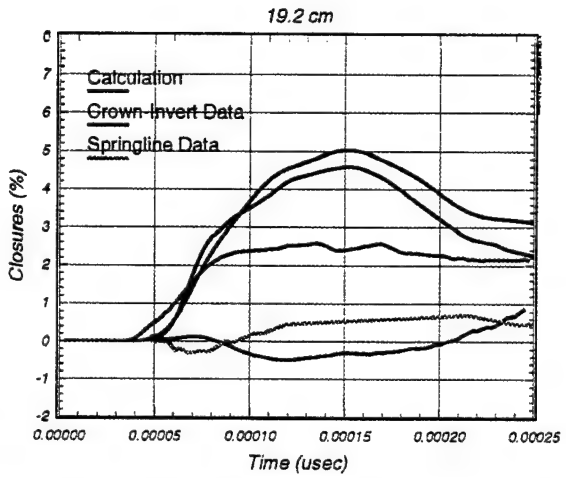


(b) Closures at the 19.2 cm tunnel.

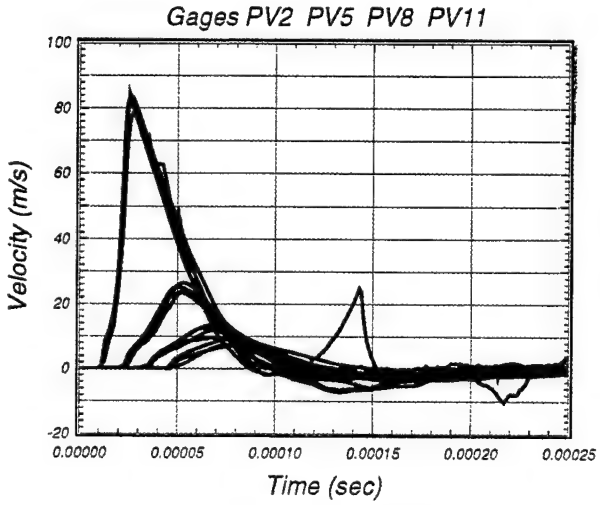


(c) Velocity histories at four gage locations.

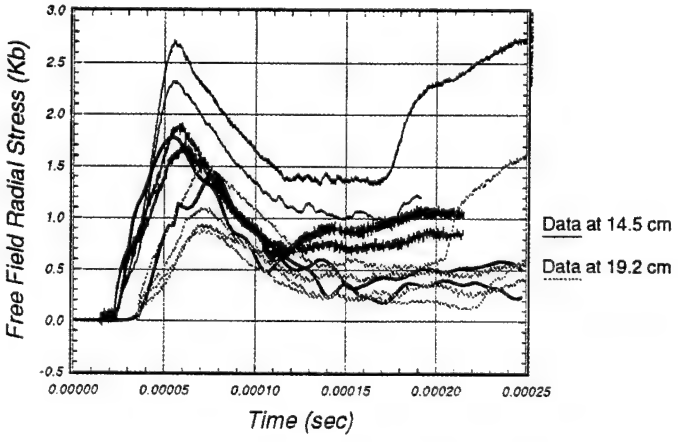


(d) Stress histories at two gage locations.

Figure 1-8. Modeling brittle damage provides more late-time springline closure than the calculations without damage. Here we modeled viscoplasticity near the source, but not near the tunnels.

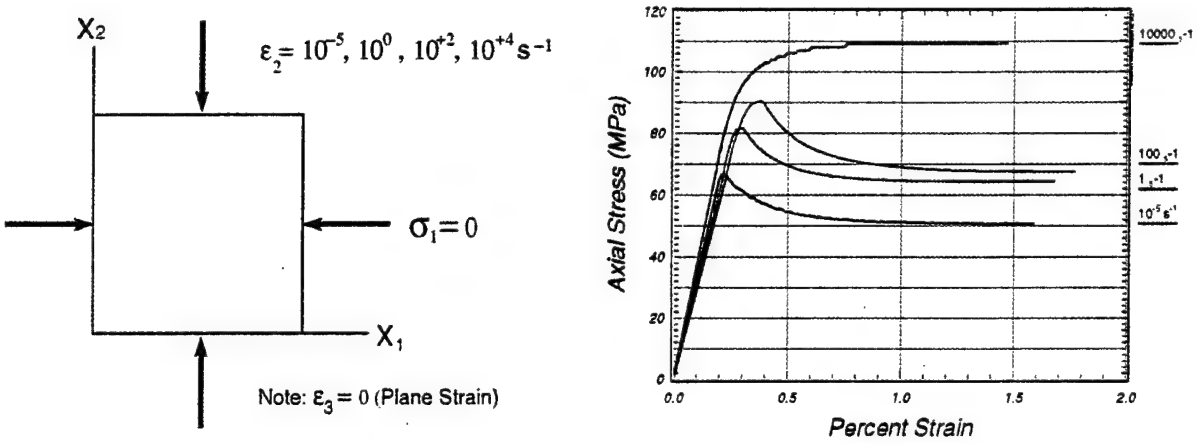


(a) Problem definition. (b) Simulation results.

Figure 1-9. This unconfined plane strain simulation is intended to represent conditions at the tunnel springline. Note that little softening is calculated by the damage model.

more physically based anisotropic model which includes the cross effect.

There are two points to note concerning the combined effects of viscoplasticity and damage. First, viscoplasticity increases the free-field stress histories, while damage, if anything, decreases the late-time stress histories. Second, modeling viscoplasticity near the tunnels tends to open the springlines, while modeling damage tends to close the late-time springlines. Perhaps adjustments in our damage model, or our fits to laboratory data, would allow for early-time closure, counteracting the opening effects of modeling viscoplasticity near the tunnels. To support this statement, consider the single element plane strain simulation, unconfined in one direction, shown in Figure 1-9. This calculation was part of the PTM calculators benchmark series and was intended to simulate the conditions at the springline. Note that our model predicts very little softening, particularly as the strain-rate increases. One suggestion is that modeling more severe softening might result in early-time springline closure, in better agreement with the measured data.

No laboratory test data is available to fit the softening response under these conditions. It seems reasonable to model more severe softening because we calculate volume expansion in this benchmark problem. In general, conventional laboratory tests indicate that volume expansion is usually accompanied by severe softening. This benchmark problem and additional SWAT simulations should be re-examined once a more physically based anisotropic model is developed.

We also recommend examining and displaying the calculated contours of damage near the source and tunnels for comparison with the post-test swat cross sections reported by Klopp *et. al.* (1995). One example cross-section is reproduced in Figure 1-10. SRI concludes that one apparent damage mechanism for the tunnels is shear faults and/or cracks extending away from the springlines. "Rubble zones" form at the springlines which intrude on the tunnel to cause springline closure. We interpret these crack patterns to mean that modeling damage

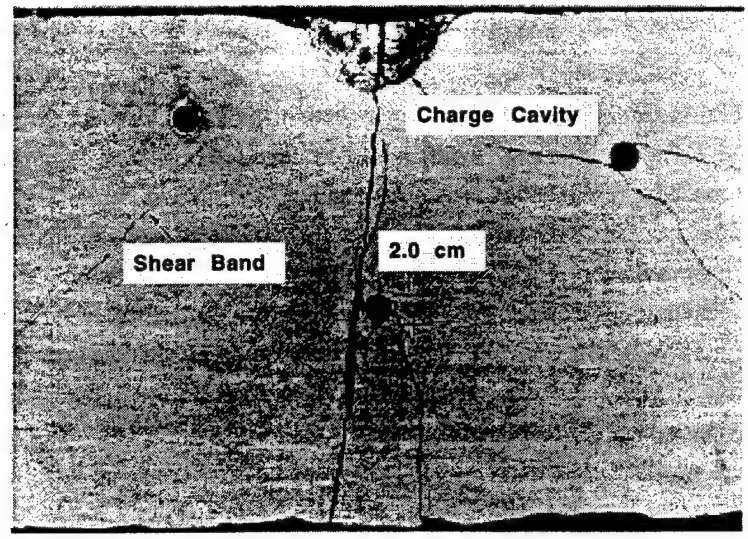


Figure 1-10. SWAT cross-section showing post-test damage near the source and tunnels.

near the springlines is critical to obtaining springline closure. Thorough correlation with the SWAT tests should include measured and predicted damage patterns, as well as velocity, stress, and closure histories.

## 1.4 VISCOPLASTIC MODEL BEHAVIOR.

Modeling rate effects with viscoplasticity significantly affects the SWAT computational results, particularly the springline closures. Hence it is important to understand the overall behavior of the model and how well it fits available test data. The behavior of the viscoplastic model under uniaxial and triaxial loading conditions is not reported in the literature, so a overview is presented in this section.

A review of high strain rate test data available in the literature indicates that the peak stress obtained from Hopkinson split pressure bar tests increases with strain rate. Data for various types of rock from Handin and Friedman (1976) is reproduced in Figure 1-11. Note that the strength for Solenhofen limestone increases exponentially with $log(\dot{\epsilon})$, where $\dot{\epsilon}$ is the strain rate. This is readily apparent above rates of about 100/s. On the other hand, some materials like basalt and tuff exhibit a linear relation between strength and $log(\dot{\epsilon})$. Hence a rate-dependent model should be flexible enough to capture this wide range in behavior.

Viscoplastic models are typically used to model rate effects such as those previously shown in Figure 1-11. Duvaut-Lions type viscoplastic models are easy to implement into existing cap models. In general, no modifications need to be made to the plasticity algorithm; the viscoplastic implementation is separate from, and follows, the plasticity algorithm. However, the most basic Duvaut-Lions model does not provide much flexibility in fitting data because it is a single parameter model. The original constitutive formulation is attributed to Duvaut and Lions (1972). It was extended to three dimensions and applied to multi-surface cap

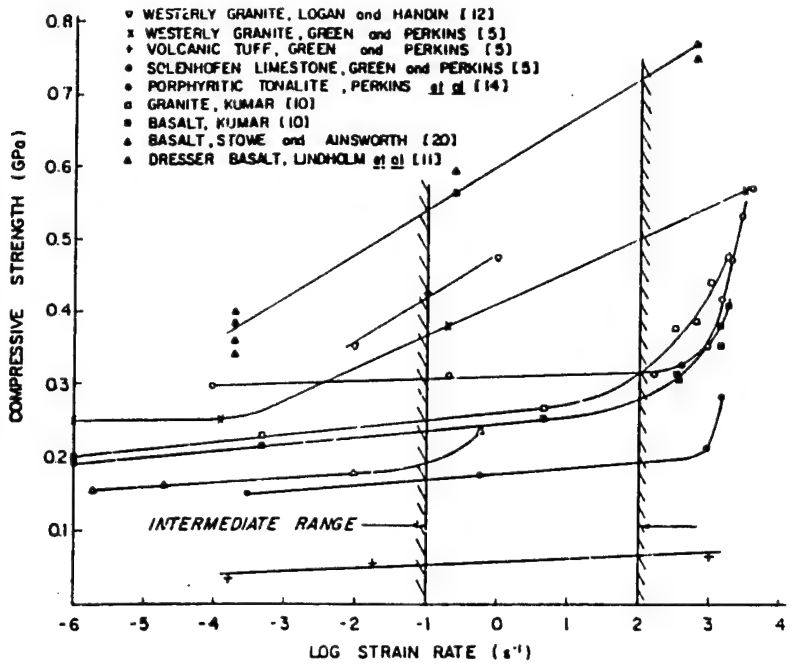


Figure 1-11. High strain rate data for rocks indicating an increase in strength with strain rate (Handin and Friedman, 1976).

models by Simo *et. al.* (1988). Their viscoplastic model requires the input of a single parameter, $\eta$, called the fluidity parameter.

### 1.4.1 Single-Parameter Model.

Some examples of good and poor fits to laboratory test data are given here to examine the overall behavior of the single-parameter Duvaut-Lions model. A good fit of the Duvaut-Lions model to Solenhofen limestone data from Hopkinson bar tests (Green, 1969) is shown in Figure 1-12. The single parameter Duvaut-Lions model corresponds to $n = 1$ solution: the parameter $n$ will be discussed in subsequent paragraphs. Although the Duvaut-Lions model fits the Solenhofen limestone data well, it would not provide a good fit to all rock data previously shown in Figure 1-11. For example, a poor comparison with concrete data is shown in Figure 1-13b. The model provides more strength enhancement in tension than in compression, in qualitative agreement with the data. However, the quantitative fit of the model to data is poor for this material. The Duvaut-Lions curves are 'steeper' than the data at high strain rates. The concrete data figure was reproduced from Ross *et. al* (1992). The data of interest are represented by the symbols: the lines represent various analyses from (Ross, 1992) that should be ignored for our purposes.

A limited amount of high strain rate data is available in the literature for stress states other than uniaxial stress or strain. Solenhofen limestone data (Brown, 1972) for a Hopkinson bar enclosed in a pressure vessel are reproduced in Figure 1-14. There is a 55% increase in strength at a confining pressure of 30 MPa, but only a 38% increase in strength at a confining pressure of 10 MPa. The rate effect increases with confining pressure for this material.

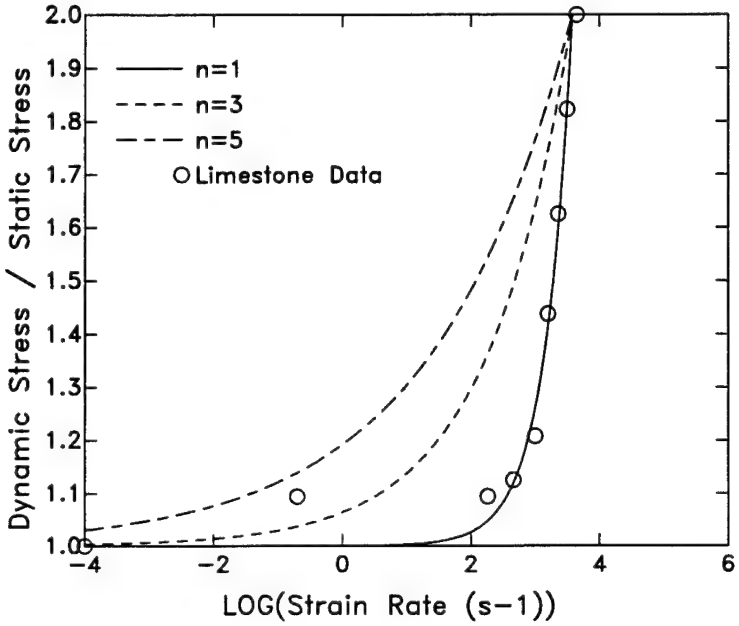


Figure 1-12. Good fit of the single parameter Duvaut-Lions ($n = 1$) model to Hopkinson bar data for Solenhofen limestone.

The general behavior of the Duvaut-Lions cap model implementation under triaxial stress conditions is shown in Figure 1-15. Without the cap, the peak stress predicted with the viscoplastic model appears to lie on a 'shifted' plasticity surface. The square symbols are the peak stresses attained in viscous TXC simulations with confining pressures of 0, 25, 50, and 100 MPa. These same computational points are replotted in Figure 1-16a versus confining pressure rather than pressure, and are labeled 'dynamic'. Also plotted for comparison are the corresponding strengths obtained with rate-independent simulations, labeled 'static'. This figure indicates that as the *confining pressure increases*, the predicted *rate effect decreases* on a percentage basis. This trend is more readily apparent in Figure 1-16b in which the computational points are plotted as the ratio of the dynamic to static strengths. This is opposite the qualitative trend previously shown for Solenhofen limestone data in Figure 1-14.

One point to note is that although the peak stress appears to lie on a shifted plasticity surface, the stress-strain curve would not be the same as that predicted with a shifted surface. The stress state calculated with viscoplasticity lies outside the failure surface. The stress-strain curve calculated with viscoplasticity is nonlinear once the stress state exceeds the plasticity surface (which does not shift), whereas the stress-strain curve calculated by shifting the plasticity surface would be linear.

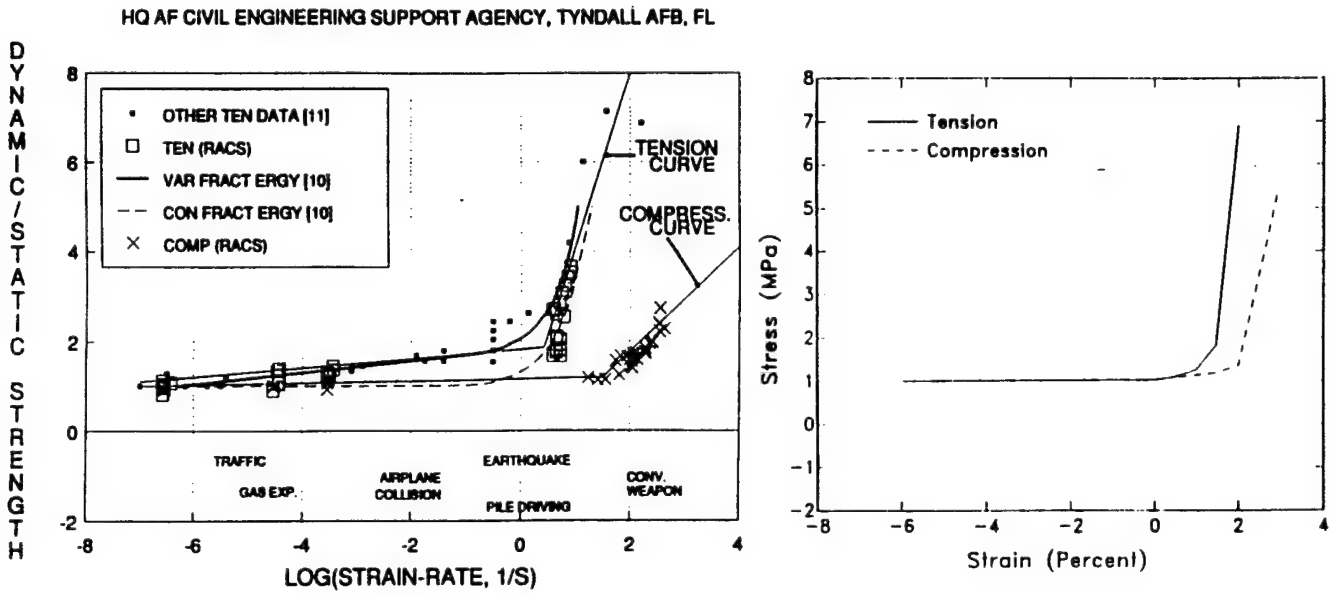


(a) Data.

(b) Viscoplastic model.

Figure 1-13. Poor comparison of the single-parameter Duvaut-Lions smooth cap implementation to concrete data ($n = 1$).

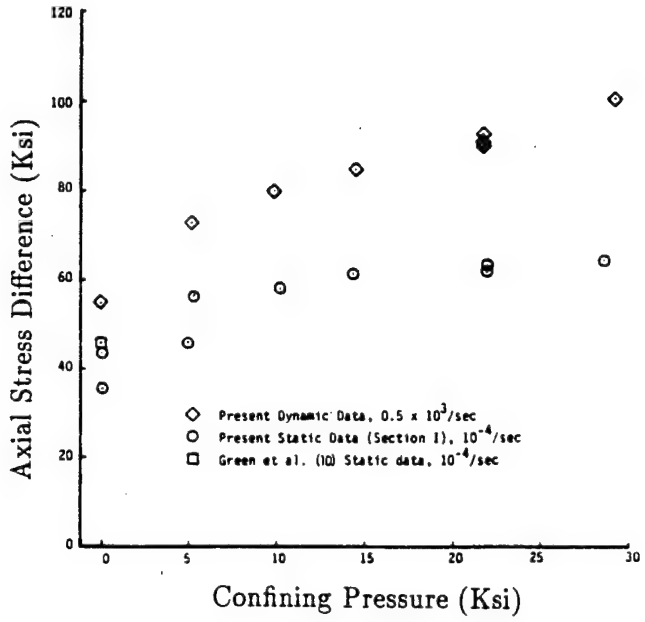


Figure 1-14. The rate effect increases with confining pressure for Solenhofen limestone data (Hopkinson bar enclosed in a pressure vessel).

### 1.4.2 Strain-Rate Dependent Extension.

These comparisons indicate that not all aspects of high strain rate data are fit well and with the desired flexibility. To provide more flexibility in fitting the data, we extended the Duvaut-Lions implementation to two parameters, effectively making the fluidity parameter a function of strain rate. As a result of this extension, we obtained good comparisons with tensile and compressive Hopkinson bar data, as shown in Figure 1-17. An overview of the extension is given in Appendix B.

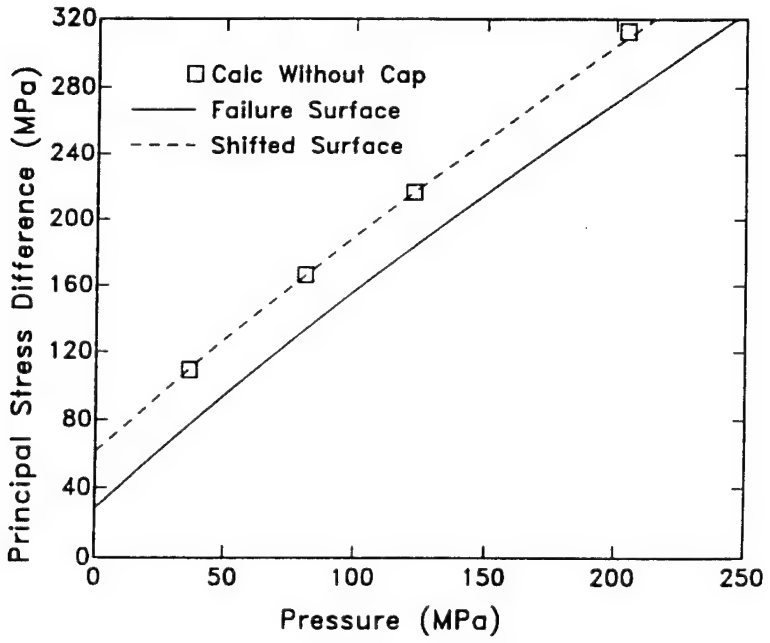


Figure 1-15. The peak stress attained with the Duvaut-Lions smooth cap implementation appears to lie on a 'shifted' plasticity surface.

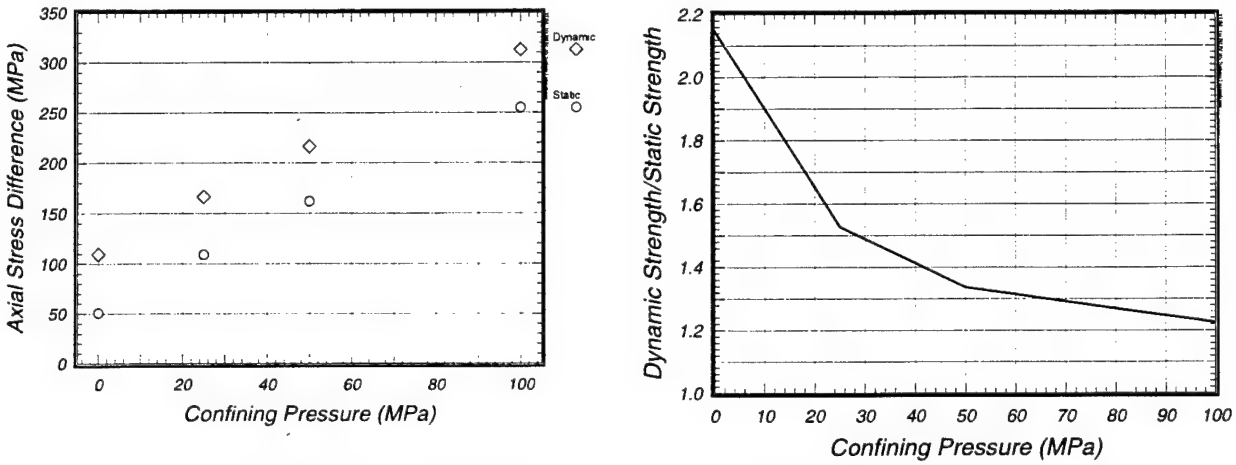


(a) Axial stress difference.

(b) Strength ratio.

Figure 1-16. The rate effect decreases with confining pressure for the Duvaut-Lions smooth cap implementation.

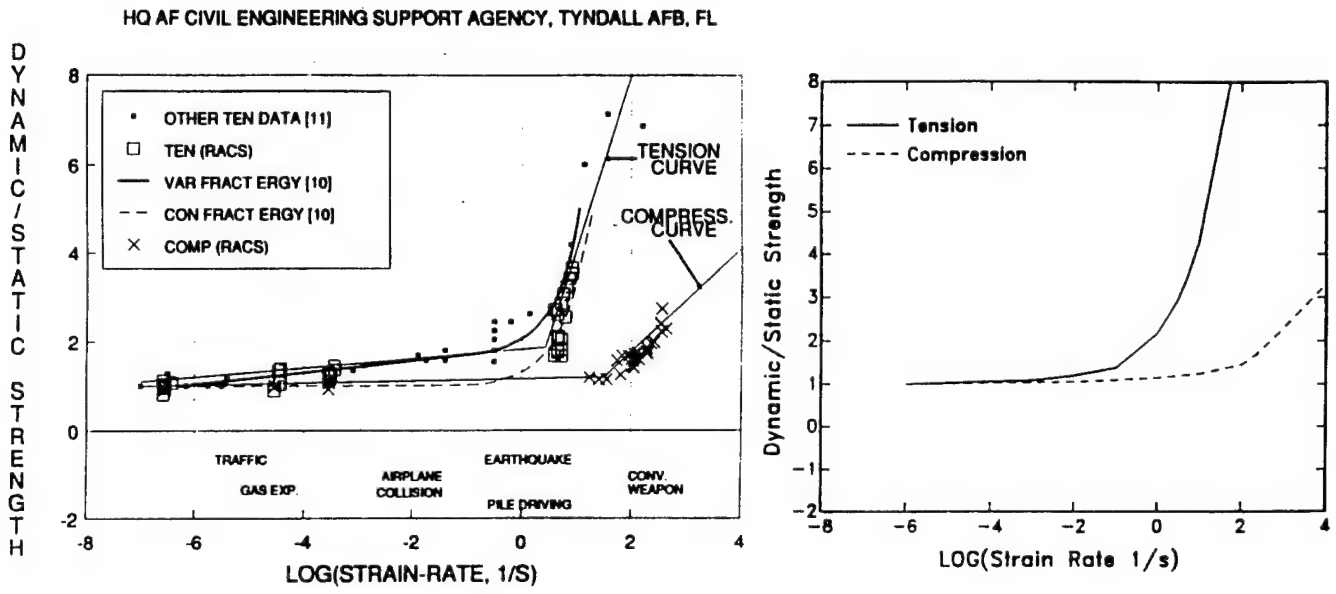


(a) Data.

(b) Viscoplastic model.

Figure 1-17. Good comparisons of the strain-rate dependent viscoplastic model with concrete data ($n = 5$).

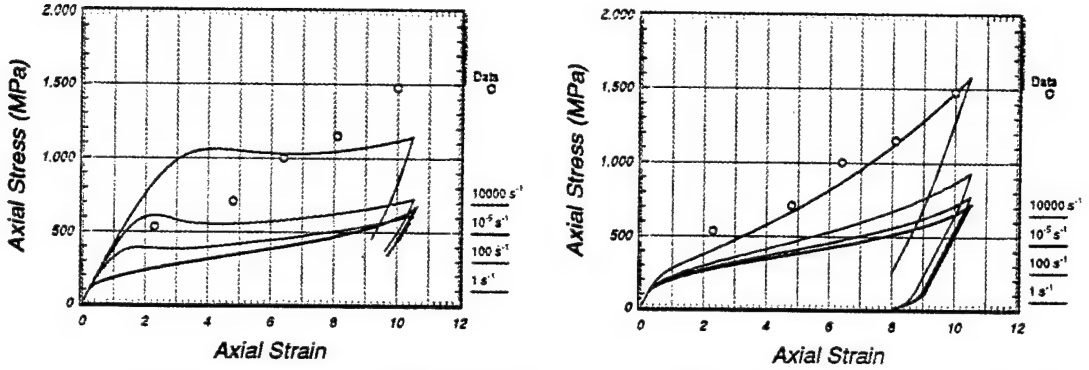


(a) Pressure-independent model. (b) Pressure-dependent model.

Figure 1-18. The pressure-dependent viscoplastic model fits Salem limestone Hugoniot data better than the pressure-independent model.

### 1.4.3 Pressure-Dependent Extension.

In general, the original and modified Duvaut-Lion models just described provide a good fit to Hopkinson bar data for a variety of geological materials, but not to Hugoniot data for Salem limestone, as shown in Figure 1-18a. To provide a better fit, we added pressure dependence to the strain-rate dependent fluidity parameter to model greater rate effects at higher pressures. Hence we are effectively modeling greater rate effects on the cap than on the shear plasticity surface. Good agreement between the pressure-dependent model and Hugoniot data for Salem limestone is shown in Figure 1-18b. Details of the pressure-dependent model are given by Murray and Lindberg (1996).

One might think that we could model different rate effects on the cap and shear failure surface by implementing *separate pressure-independent* viscoplastic formulations for the cap and shear failure surface. Although this would allow one to separately fit the Hugoniot data and Hopkinson bar data, a desirable feature, it would not provide a better qualitative fit to the Hugoniot data shown in Figure 1-18a. A pressure-independent fluidity parameter would remain constant through-out each simulation. Hence we could obtain a different fit than previously shown in Figure 1-18a, but it would not be a better qualitative fit. To obtain a better fit to the Hugoniot data, we need to model less rate effects at low axial strain (or pressure) and more rate effects at high axial strain (or pressure) than modeled with the pressure-independent formulation in Figure 1-18a. This is accomplished by varying the fluidity parameter as a function of pressure.

### 1.4.4 Inertial Effects.

One current issue is whether the sharp increase in strength with strain rate commonly observed in Hopkinson bar tests is a rate effect or inertial effect. In fact, different types of high strain rate tests give different results at high strain rates, indicating that inertial effects may be less significant in some tests than others. For example, Green and Perkins (1969) used a compressive split Hopkinson bar, and measured a 100% increase in strength for Solenhofen limestone at loading rates of about 5000 $s^{-1}$. Lipkin, Grady, and Cambell (1977) used a torsional split Hopkinson bar, and also measured about a 100% increase in shear strength at loading rates of about 600 $s^{-1}$. On the other hand, Young and Dubugnon (1977) used a reflected shear wave technique, and determined that the dynamic shear strength for Solenhofen limestone, at loading rates up to $10^6$ $s^{-1}$, did not exceed the static strength by more than 25%.

Two approaches for resolving this issue are computationally (mesh up a Hopkinson bar and predict its response) and experimentally. Lateral accelerations of a Hopkinson bar specimen were measured by Malvern *et. al.* (1986) and Tang *et. al.* (1992). Malvern concluded that lateral inertia confinement becomes significant at strain rates of about 100 $s^{-1}$. However, Tang concluded that lateral accelerations were too small to account for the factor of two enhancement of the dynamic compressive strength above the static strength, suggesting that inertial effects are insignificant for strain rates on the order of 100/s. This is an issue that should be resolved in future efforts.

# SECTION 2

# JOINT MODEL AND STACK OF BRICK SIMULATIONS

## 2.1 JOINT MODEL OVERVIEW.

We use a rate-dependent slideline approach for explicitly modeling rock joints. To provide a better fit to joint normal compressibility data, we modified the DYNA3D slideline formulation to make the normal stiffness a function of the penetration depth. A good fit of the nonlinear joint model to normal compressibility data is shown in Figure 2-1. To provide more flexibility in fitting joint shear data, we modified the formulation to make the shear stiffness independent of the normal stiffness. The joint model also includes a rate-dependent Coulomb friction model in shear, as discussed for slidelines in the DYNA3D Users Manual (Whirley and Engelmann, 1993)

## 2.2 JOINT RATE EFFECTS.

All PTM calculators ran a benchmark problem to exercise the joint in shear. Two blocks of intact rock separated by a diagonal joint are subjected to normal displacements. The displacement path from Simons (1993) is reproduced in Figure 2-2. Each triangular block was modeled with a single element. Computational results with and without joint rate effects are given in Figure 2-3. They indicate that the joint rate model lowers the joint shear stress at high strain rates. No measured data was available for verifying our joint rate model. Future efforts should examine available test data to determine if joint rate effects are important, and, if so, determine the availability of joint rate data for fitting and validating the model.

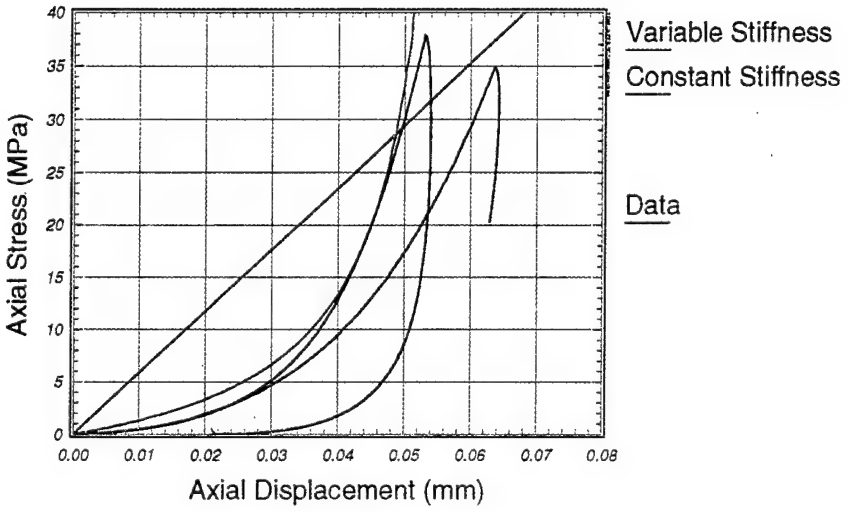


Figure 2-1. The nonlinear joint model fits normal compressibility data better than the linear model.

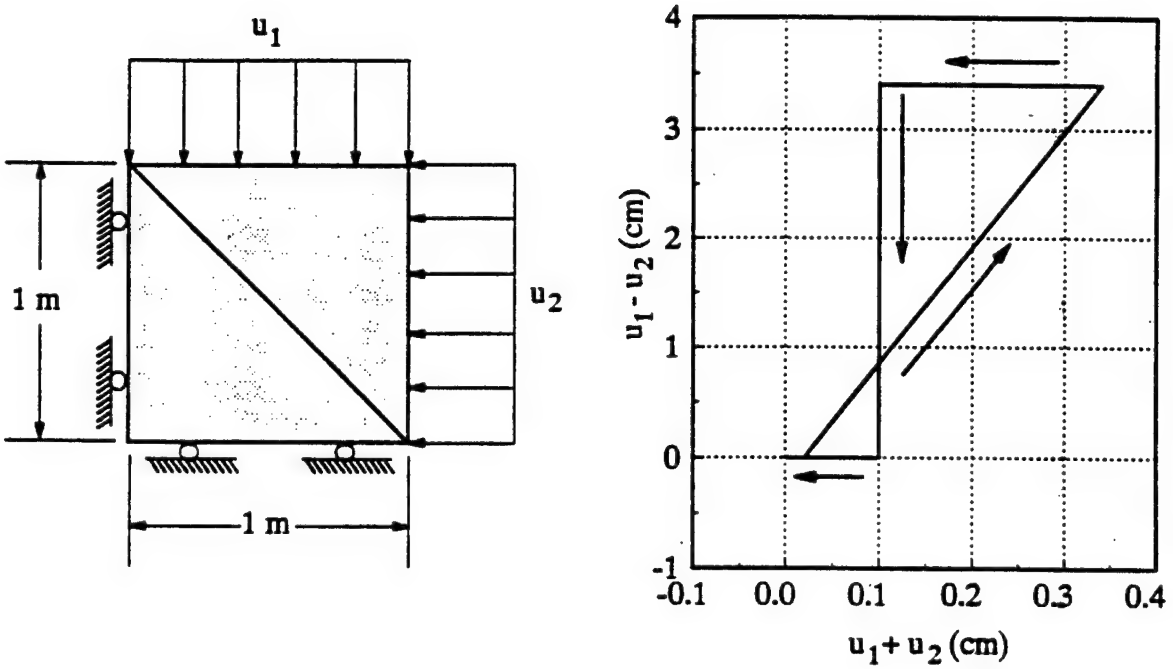


Figure 2-2. Joint shear benchmark geometry and loading.

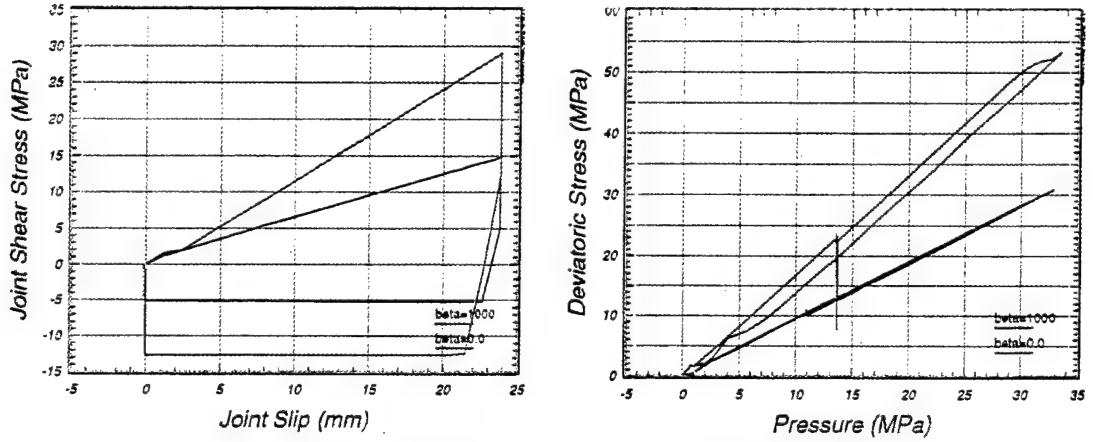


(a) Joint behavior. (b) Limestone behavior.

Figure 2-3. Preliminary joint sliding calculations with and without rate effects ($\beta = 100$ indicates rate effects).

## 2.3 STACK OF BRICKS COMPUTATIONAL SUMMARY.

The Mighty North 1 (MN-1) phenomenology test was designed to investigate the effects of joints on tunnel deformation, and to provide data for benchmarking and model validation. It consists of a tunnel in jointed limestone subjected to a cylindrically-divergent ground shock load. The compressional properties and damage mode of the jointed limestone "stack of bricks" (SOB) arrangement were measured by ARA for benchmarking calculations (Chitty and Blouin, 1995). The stack of bricks test configuration is given in Figure 2-4.

Using our linear joint and intact rock models, we performed some preliminary plane strain calculations to verify our SOB generation scheme and intact/joint model behaviors. Although the cross-section of each brick is nominally 2-inch by 2-inch, slight variations in the size of each brick cause vertical and horizontal gaps to form in the SOB. Using the mesh generator PATRAN, we successfully developed a system to *scale* each brick model to form a stack of irregular bricks. PATRAN conveniently allows the user to create one brick, then *scale* and *translate* each brick to form a stack of irregular bricks. The *scale* factors are based on a random number from a normal distribution, and an assumed standard deviation. The *translate* factors are calculated by placing each brick on the highest of the two bricks beneath it. The bottom row of bricks sits on a steel platten, with no gaps between the bricks and platten.

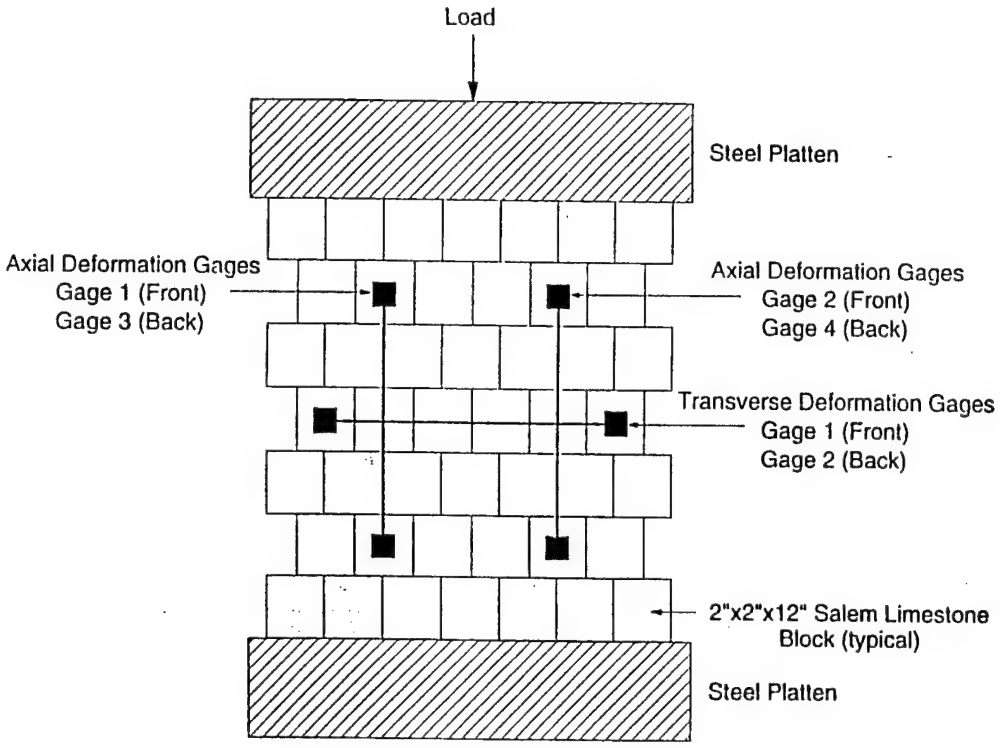


Figure 2-4. Stack of bricks layup and gage locations.

Our preliminary plane strain calculations indicate that the predicted damage pattern for the compressional tests is sensitive to the presence of irregular gaps. Damage contours calculated for regular (no gaps) and irregular (with gaps) bricks are shown in Figure 2-5 and indicate that modeling irregular gaps causes asymmetry in the computed damage pattern. Modeling irregular gaps also produces early-time nonlinearities in the stress-strain response, as shown in Figure 2-6. Asymmetry of the measured damage pattern, and early-time nonlinearity of the measured stress-strain response were also observed in the test.

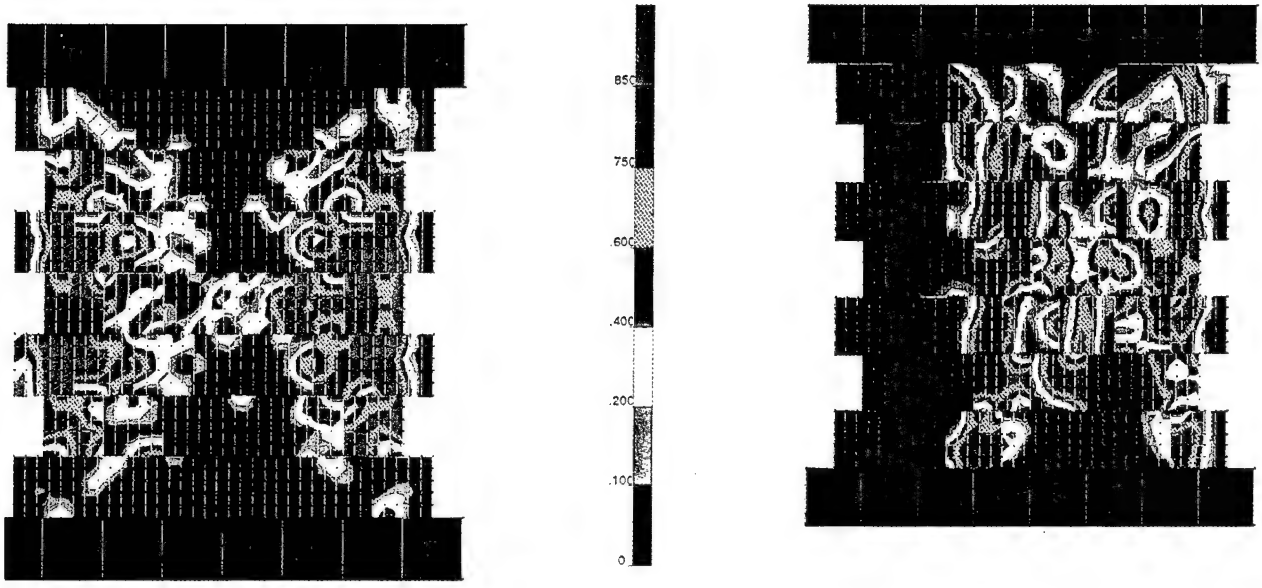


(a) Without gaps.

(b) With irregular gaps.

Figure 2-5. Modeling irregular gaps produces asymmetric damage patterns in the preliminary "stack of bricks" simulation. An asymmetric damage pattern was also observed in the stack of bricks test.

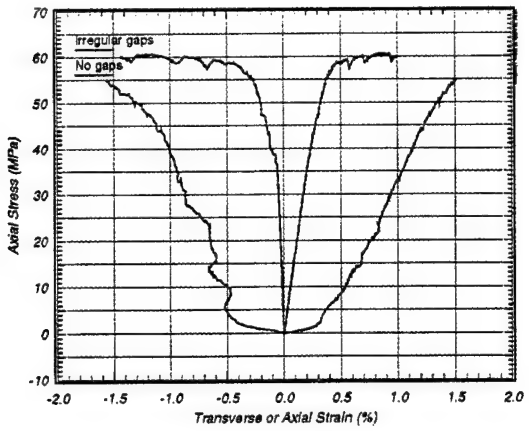


Figure 2-6. The preliminary SOB stress-strain history calculated with initial gaps is more nonlinear than that calculated without initial gaps.

These plane strain calculations were intended to be preliminary runs to check out our irregular SOB generation scheme and the intact/joint model behaviors before running more time consuming and costly three-dimensional calculations. To complete verification of our joint model, we recommend running all calculations with the nonlinear joint model, including horizontal as well as vertical gaps, and analyzing the effect of boundary conditions on the predicted response, including rotation of the plattens. Another possibility is setting up the irregular brick distribution to match that in the SOB test. ARA measured each brick dimension and noted its placement in the SOB. In this way, we can check our predicted damage pattern against the measured damage pattern observed in the test, as well as the compare measured versus calculated stress-strain responses.

Once we verify our model for this particular stack, additional parameter studies in preparation for MN-1 could include:

- Three-dimensional calculations versus plane strain calculations.
- The effects of varying joint shear stiffness, as well as varying joint normal stiffness, on the predicted response.
- The effects of average gap size, gap standard deviation, and brick stacking pattern on stack strength. We want to determine if stack strength is primarily determined by average gap size and standard deviation regardless of the stacking pattern, or if the stacking pattern plays a significant role in strength. This is important because we will not know the stacking pattern in the MN-1 test, only the average gap size.
- The effects of a joint rate model on the predicted response at high strain rates.

# SECTION 3

# SUMMARY AND LESSONS LEARNED

The three-invariant smooth-cap model with damage provides good fits to quasi-static and high strain rate data for limestone, and correlates well with SWAT data. However, the *predictive* capability of the model has not been established for tunnel response applications, because only a few static and dynamic laboratory tests have been analyzed. To establish a predictive capability, we recommend the following iterative procedure:

1. Enhance the formulation of the model. At this time, this includes additional damage model development, understanding the differences between inertial and rate effects, and examining alternatives to viscoplasticity.

2. Verify the formulation through correlations with dynamic tunnel test data, such as SWAT. We recommend comparing contours of calculated damage with post-test observations of the fault/cracking pattern, as well as comparing measured and calculated free-field and tunnel closure histories. Additional parametric studies should also be performed to determine the sensitivity of tunnel response to model parameters or specific formulations (like damage versus rate effects). At this time, we reserve judgement on the sensitivity of dynamic tunnel response to model parameters until the damage modeling, rate effects, and inertial effects issues are more clearly resolved.

3. Perform pre-test predictions and/or blind post-test predictions of dynamic tunnel tests performed in the laboratory or field. *Accurate predictions are the only means of validating a code.* Post-test correlations should only be used for identifying improvements to the physical basis and/or implementation of the model.

No information was available in the literature describing the behavior of the single-parameter Duvaut-Lions viscoplastic model under general loading conditions. To understand the model, we examined its behavior under conditions of uniaxial stress, uniaxial strain, and triaxial compression, and compared the behavior to geological/concrete data available in the literature.

We learned that the single-parameter Duvaut-Lions model (viscoplastic) does not provide adequate flexibility in fitting a wide variety of high strain rate geological data over various regimes (uniaxial stress, uniaxial strain, triaxial stress). We improved the models flexibility in fitting Hopkinson bar and Hugoniot data by extending the model to multiple parameters. These extensions make the effective fluidity parameter a function of pressure and strain-rate. The extensions are based, in part, on analytical comparisons between Duvaut-Lions and Perzyna-type models.

Peak velocities, stresses, and closures calculated without rate effects were low in comparison with measured test data. To improve comparisons with the test data, we used the extended viscoplastic model in our SWAT calculations. Although our calculated free-field stress and velocity histories compared well with the measured histories, the calculated springlines opened

slightly whereas the measured springlines closed slightly. The only way we were able to calculate springline closure was to model rate effects near the source, but not near the tunnels. We note that, near the source, the pressure is high and the stress state lies on the cap. Near the tunnels, the pressure is low and the stress path encounters the shear failure surface.

Two approaches could be taken to attempt better agreement with the springline closures. The first approach is to continue to tune our fits and/or viscoplastic formulation. The general approach of the PTM group calculators was to model different rate effects on the cap than on the shear failure surface, *i.e.* strong rate effects on the cap, but minimal rate effects on the shear failure surface. The assumption here is that different physical processes are taking place: volume crushing on the cap, and shear failure on the failure surface. However, two modifications were made to the viscoplastic model to get it to agree with laboratory data suggesting that viscoplasticity may not be the best method of modeling these different mechanisms. In fact, the general behavior of the original viscoplastic (before modifications) was that rate effects *decreased* with pressure, at odds with the desired trend.

The second approach is to examine alternatives to viscoplasticity. One example is use a nonlinear Mie-Gruniesen model in place of a constant bulk modulus model. Comparisons with measured particle velocity records from Hugoniot tests should indicate whether pore collapse rate effects still need to be modeled. Although no data was available for Salem limestone at very high compaction levels, many geological/concrete materials exhibit a stiffening behavior at high pressure. Such behavior is simulated by the Mie-Gruniesen model, but not by the constant bulk modulus model. We recommend this approach for future tunnel response calculations, at least for comparison with viscoplastic model results.

These efforts show that no single set of laboratory test data can be used to formulate and verify a comprehensive, three-dimensional rate-dependent model. We want to formulate models with the right trends over a range in loading regimes. This can be accomplished by examining a wide variety of geological/concrete materials and tests, such as tensile and compressive Hopkinson bar, plate-slap Hugoniot tests, and divergent flow tests. Once the *general* behavior of a model is understood, then the *specific* behavior of the model can be verified for a material of interest, such as Salem limestone. This same approach, general formulation then specific fits, can be used when developing damage models.

We implemented a scalar anisotropic damage model in order to to simulate strain-softening and modulus reduction in the tensile and low-confining pressure regimes. The model is loosely based on research by Ju (1989). The motivation for implementing an anisotropic model instead of an isotropic[1] model is that damage in geological materials is directional in nature. Anisotropy adds more physics to the model, without requiring any additional laboratory data to fit the model.

We used the anisotropic damage model in our SWAT calculations, with and without modeling viscoplasticity. We obtained our best correlations with the measured SWAT histories using

[1]Interested readers should refer to Murray and Lewis (1995) for a description of the isotropic damage formulation that APTEK previously implemented into DYNA3D on DNA's Conventional Weapons Effects (sc cwe) Program. This model has sucessfully been used to *predict* damage to reinforced concrete bunkers subjected to internal detonations.

a combination of brittle damage and viscoplasticity modeled near the source. Modeling damage and viscoplasticity tend to have counteracting effects on some of the calculated histories. In general, viscoplasticity increases the free-field stress histories, while damage decreases the late-time stress histories. Modeling viscoplasticity near the tunnels opens the springlines, while modeling damage tends to close the springlines, at least at late-time.

Although our SWAT correlations are reasonable, we recommend further anisotropic damage model development for two reasons. First, the model simulates little strain-softening under conditions of "unconfined plane strain," such as occurs near the springline closure. We would like to determine if more severe softening under these conditions allows for early-time, rather than late-time, springline closure, in better agreement with the opening-closing response of the measured data. Second, the model does not simulate a "cross effect' between degradation in one principal direction and degradation in another, hence the physical basis of our implementation is not satisfactory. Future efforts should examine the combinations of scalar damage criteria and projection operators that will realistically produce a cross effect. Once the general anisotropic formulation is verified against test data available in the literature, additional SWAT parametric studies should be performed, with and without the proposed Hugoniot and viscoplastic models.

At the beginning of the current program, predictions were made with geological models with limited physics; damage (softening and modulus reduction) was neglected while rate effects were modeled in a very approximate manner. Thus most differences between the measured and calculated histories were initially attributed to how we modeled rate effects. The result of this *sequential* approach is that modeling rate effects received more attention than modeling damage effects. However, subsequent damage model calculations and post-test observations of the SWAT fault/cracking patterns, indicate that modeling damage may play an important role in correlating with the SWAT data. For future efforts we recommend a more global approach in which known physical mechanisms are modeled before parametric studies are performed and model sensitivities are concluded.

Efforts to develop and verify a jointed rock model are still in progress. We sucessfully developed a nonlinear joint model which fits normal compressibility data well. Preliminary plane-strain "stack of brick" simulations were performed to understand the effects of joint gaps on predicted damage patterns and stress-strain curves. Irregular gaps cause asymmetry in the predicted damage pattern and nonlinearity of the stress-strain response. Future efforts should include three-dimensional calculations for comparison with the measured stress-strain curves and post-test damage pattern, to verify our jointed rock model. However, as previously stated, accurate *predictions* are the only means of validating a code. Future calculations should include "blind" post-test MN-1 predictions and field test predictions. Unlike the manufactured joints in the MN-1 tests, natural rock joint patterns will be random (and unknown) in field tests, which will be a challenge for future efforts.

## SECTION 4

## REFERENCES


Brown, W.S. , S.R. Swanson, W.R. Wawersik, (1972). "Further Studies of Dynamic and Biaxial Loadings of Rock," Final Report to Defense Atomic Support Agency, DASA 01-71-C-0017, DNA 2887I, Feb. 1972. (UNCLASSIFIED)

Chitty, D. and S. Blouin, (1995), "Laboratory Test Data for Salem Limstone to Support Modeling of Mighty North 1," Memorandum from ARA to Precision Test Modelers, April, 1995. (UNCLASSIFIED)

Duvaut, G. and J.L. Lions, (1972), "Les Inequations en Mechanique et en Physique," Dunod, Paris, 1972. (UNCLASSIFIED)

Fossum, A.F., Pfeifle, T.W., and K.D. Mellegard, (1995) "Experimental Determination of Probability Distributions for Parameters of a Salem Limestone cap Plasticity Model," DNA-TR-94-39, RE/SPEC, Inc. (UNCLASSIFIED)

Green, S.J., and R.D. Perkins, (1969), "Uniaxial Compression Tests at Strain Rates From $10^{-4}$/sec to $10^{4}$/sec on Three Geologic Materials," Materials & Structures Laboratory, Manufacturing Development, General Motors Corporation, MSL-68-6, Defense Atomic Support Agency, NWER Susbtask SB047, DASA-2199. January, 1969. (UNCLASSIFIED)

Handin, J. and M. Friedman, (1976). "Mechanical Properties of Rocks Related To Drilling Technology," Center for Tectonophysics. Texas A&M University, Ninth Quarterly Progress Report to Sandia Laboratories, Contract No. 82-9473, Oct. 1976. (UNCLASSIFIED)

Ju, J.W., (1989), "On Energy-Based Coupled Elastoplastic Damage Theories: Constitutive Modeling and Computational Aspects," *International Journal of Solids and Structures,* Vol. 25, No. 7, pp. 803-833, 1989. (UNCLASSIFIED)

Klopp, R. W., et al., (1995), *Laboratory Tests in Support of the Underground Technology Program (*UTP*)*, SRI International technical report to Defense Nuclear Agency, DNA-TR-94-183, November 1995. (UNCLASSIFIED)

Larson, D.B. and G.D. Anderson, (1979). "Plane Shock Wave Studies of Porous Geologic Media," *Journal of Geophysical Research*, Vol. 84, No. B9, August 10, 1979, pps. 4592-4600. (UNCLASSIFIED)

Lipkin, J., D.E. Grady, J.D. Campbell, (1977), "Dynamic Flow and Fracture of Rock in Pure Shear," Energy Resources and Excavation Technology Proceedings, 18th US Symposium on Rock Mechanics, Published by CO School of Mines Press, 1977, pp. 3B2-1 to 3B2-7. (UNCLASSIFIED)

Malvern, L.E., T. Tang, D.A. Jenkins, J.C. Gong, (1986), "Dynamic Compressive Strength of Cementitious Materials," Mat. Res. Symp. Proc., Vol. 64, 1986. (UNCLASSIFIED)

Murray, Y.D. and B.A. Lewis, (1995). "Numerical Simulation of Damage in Concrete",

APTEK Inc, Colorado Springs, CO, Technical Report to DNA, DNA-TR-94-190, DNA 001-01-C-0075, Nov. 1995. (UNCLASSIFIED)

Murray, Y.D. and H.E. Lindberg (1996), "Kill Algorithms and Computational Modeling of Underground Tunnels in Intact and Jointed Rock," APTEK Technical Report, A-96-XX, APTEK Inc, Colorado Springs, CO, April 1996. (UNCLASSIFIED)

Ortiz, M., (1985), "A Constitutive Theory for the Inelastic Behavior of Concrete," *Mechanics of Materials*, North Holland, Vol. 4, No. 1, March 1985. (UNCLASSIFIED)

Pelessone, D., (1989), "A Modified Formulation of the Cap Model," General Atomics, Prepared for DNA under Contract DNA-0010086-C-0277, GA-C19579, January 1989. (UNCLASSIFIED)

Perzyna, P., (1971), "Thermodynamic Theory of Viscoplasticity," *Advances in Applied Mechanics*, Vol. 11, Academic Press, New York, 1971, pps. 313-354. (UNCLASSIFIED)

Ross, C.A., S.T. Kuenned, and J.W. Tedesco, (1992), "Effects of Strain-Rate on Concrete Strength," HQ AF Civil Engineering Support Agency, Tyndall AFB, Presented at the American Concrete Institute 1992 Spring Convention, Washington D.C., March 1992. (UNCLASSIFIED)

Sandler, L.S. and D. Rubin, "An Algorithm and a Modular Subroutine for the Cap Model," *International Journal for Numerical and Analytical Methods in Geomechanics 3,*, pps. 173-186, 1979. (UNCLASSIFIED)

Schwer, L.E. and Y.D. Murray, (1994), "A Three Invariant Smooth Cap Model with Mixed Hardening," *International Journal for Numerical and Analytical Methods in Geomechanics,* Vol. 18, 1994, pgs 657-688. (UNCLASSIFIED)

Simo, J.C., J.G. Kennedy, S. Govindjee, (1988), "Non-Smooth Multisurface Plasticity and Viscoplasticity. Loading/Unloading Conditions and Numerical Algorithms," *International Journal for Numerical Methods in Engineering*, Vol. 26, 1988, pps. 2161-2185. (UNCLASSIFIED)

Simons, D.A., (1993), "Numerical and Analytical Solutions to Benchmark Problems Related to Tunnel Mechanics," Logicon R&D Assoc, Los Angeles CA, Technical Report to DNA, 001-88-C-0046, DNA-TR-92-176, Sept. 1993. (UNCLASSIFIED)

Tang, T., L.E. Malvern, and D.A. Jenkins, (1992), "Rate Effects in Uniaxial Dynamic Compression of Concrete," *Journal of Engineering Mechanics,* Vol. 118 No. 1, Jan. 1992. (UNCLASSIFIED)

Thacker, B.H., D.S. Rhia, and L.E. Schwer, "Computational Model Comparisons with Static and Dynamic Experiments of Tunnels in Limestone," AMD-Vol. 213, Numerical Implementation and Application of Constitutive Models in the Finite Element Method, Book No. H01015, 1995. (UNCLASSIFIED)

Whirley, R.G. and B.E. Engelmann, (1993), *DYNA3D: A nonlinear, Explicit, Three-Dimensional Finite Element Code for Solid and Structural Mechanics - User Manual*, Methods Development Group, Mechanical Engineering, Lawrence Livermore National Laboratory, UCRL-

MA-107254, Rev. 1, Nov. 1993. (UNCLASSIFIED)

Young, C. , and O. Dubugnon, (1977), "A Reflected Shear-Wave Technique for Determining Dynamic Rock Strength," *International Journal of Rock Mechanics, Mineral Science, and Geomechanics,* Vol. 14, pp. 247-259, 1977. (UNCLASSIFIED)

# APPENDIX A

# FITS OF THE INTACT ROCK MODEL TO DATA

The three-invariant smooth-cap model with brittle and ductile damage provides good fits to quasi-static laboratory test data for Salem limestone as demonstrated in Figures A-1 and A-2. The data were provided by ARA (Chitty and Blouin, 1995) and RE/SPEC (Fossum *et. al.*, 1995). Both the peak stress and post-peak softening responses fit the data well.

No high strain rate laboratory tests were conducted on Salem limestone by ARA or RE/SPEC, although Hugoniot data for Salem limestone was available in the literature (Larson, 1979). The fit of our pressure-dependent viscoplastic model to this data is shown in Figure A-3a. As an alternate specification, we also fit our viscoplastic model directly to SWAT data, as discussed in Section 1.3. Stress-strain curves resulting from this fit are shown in Figure A-3b. They indicate greater rate effects than the fit to Hugoniot data shown in Figure A-3a.

The SWAT and Hugoniot data is primarily high pressure data, so the rate-dependent behavior in uniaxial stress still has to be specified. Based on a general review of Hopkinson bar data available in the literature, we assumed that strength enhancement increases by about a factor of two at high strain rates near $10^4$. This is true for Solenhofen limestone shown in Figure 1-12 and reported by Green (1969) These assumed 'fits' are given in Figures A-4 and A-5.

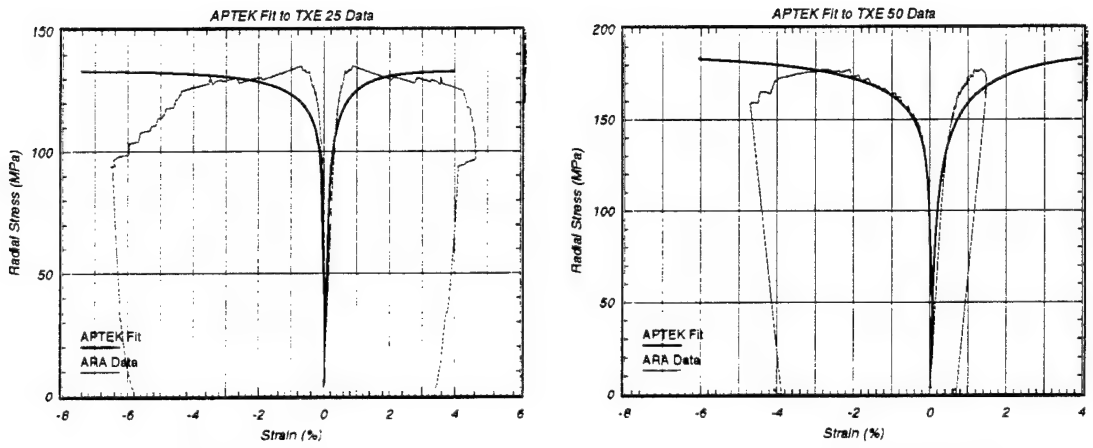


(a) 25 MPa. (b) 50 MPa.

Figure A-1. Good fits of model to triaxial extension data for Salem limestone.

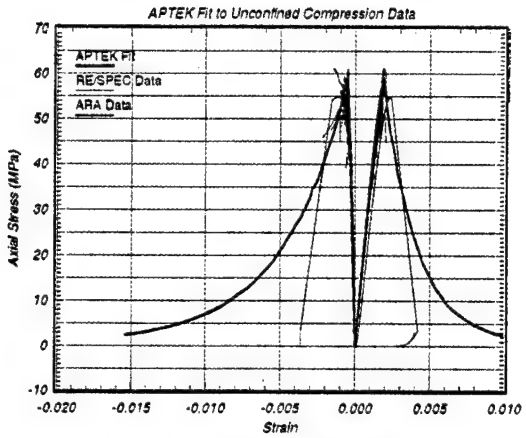


(a) Unconfined.

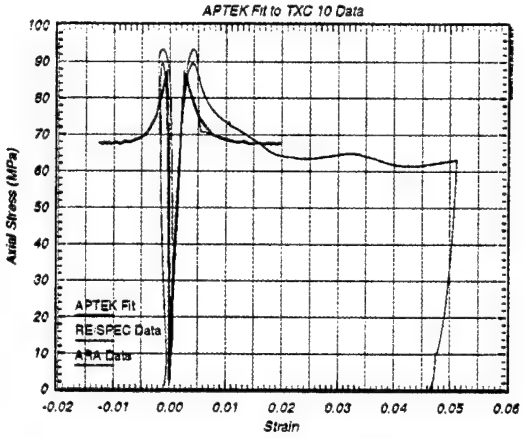


(b) 10 MPa.

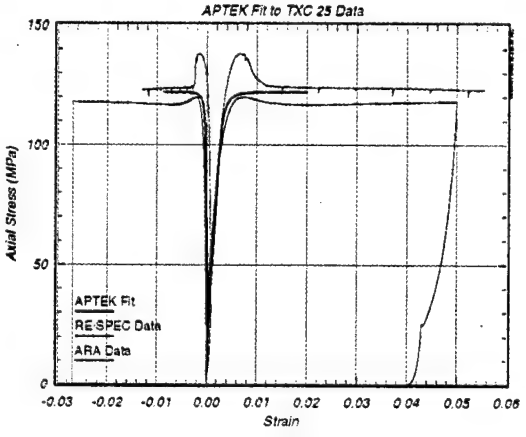


(c) 25 MPa.

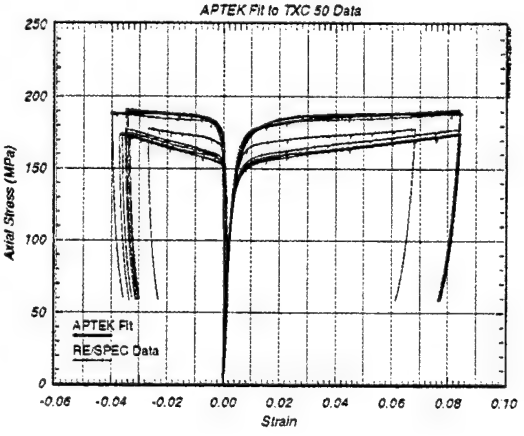


(d) 50 MPa.

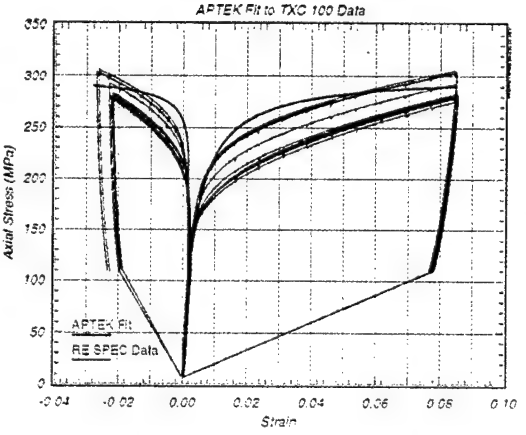


(a) 100 MPa

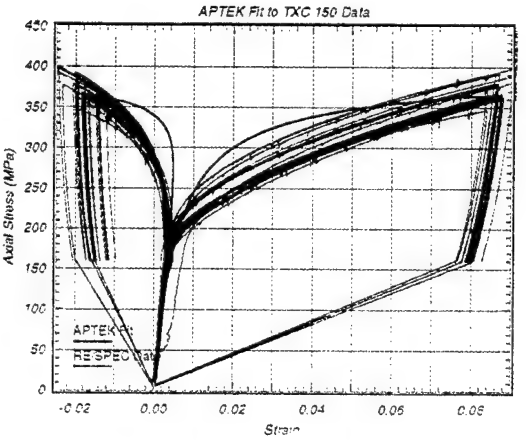


(b) 150 MPa.

Figure A-2. Good fits of model to triaxial compression data for Salem limestone

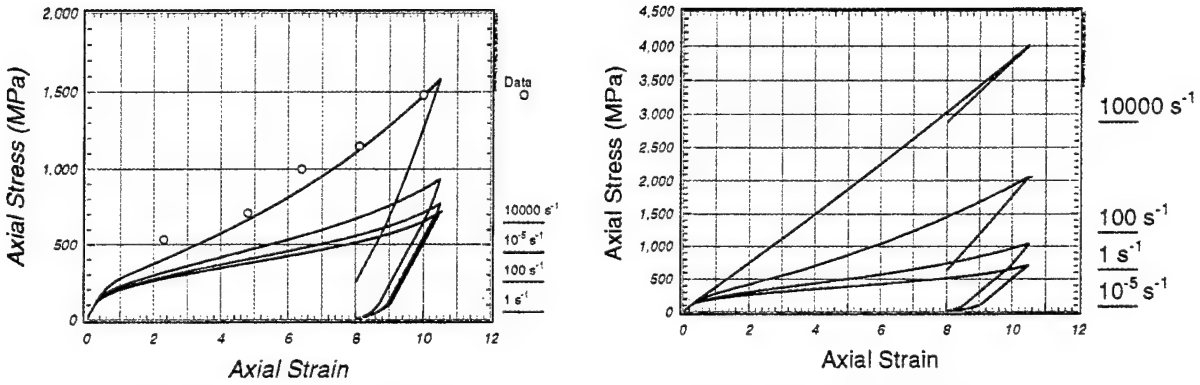


(a) Fit to Hugoniot data. (b) Fit to SWAT data .

Figure A-3. Uniaxial strain behavior of the model at four strain rates for two different fits to data.

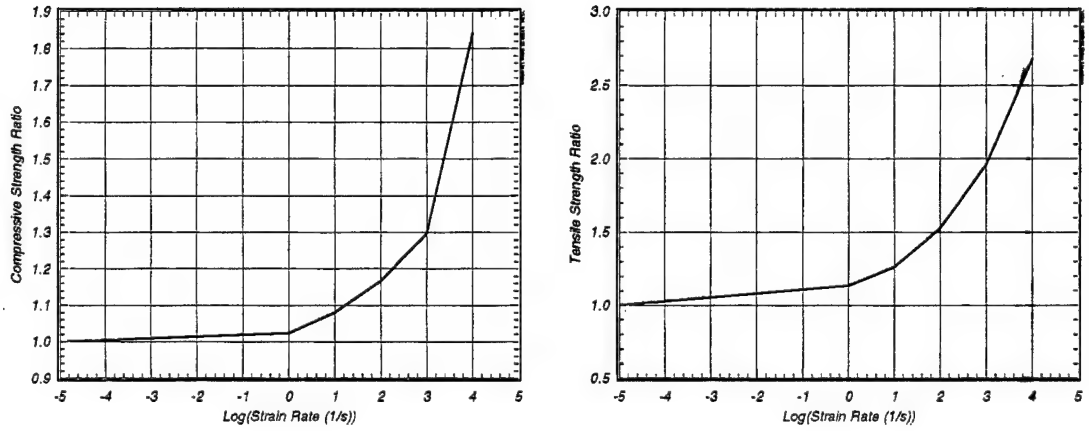


(a) Unconfined compression.

(b) Unconfined tension.

Figure A-4. Assumed strength versus strain rate behavior of model showing greater rate effects in tension than in compression.

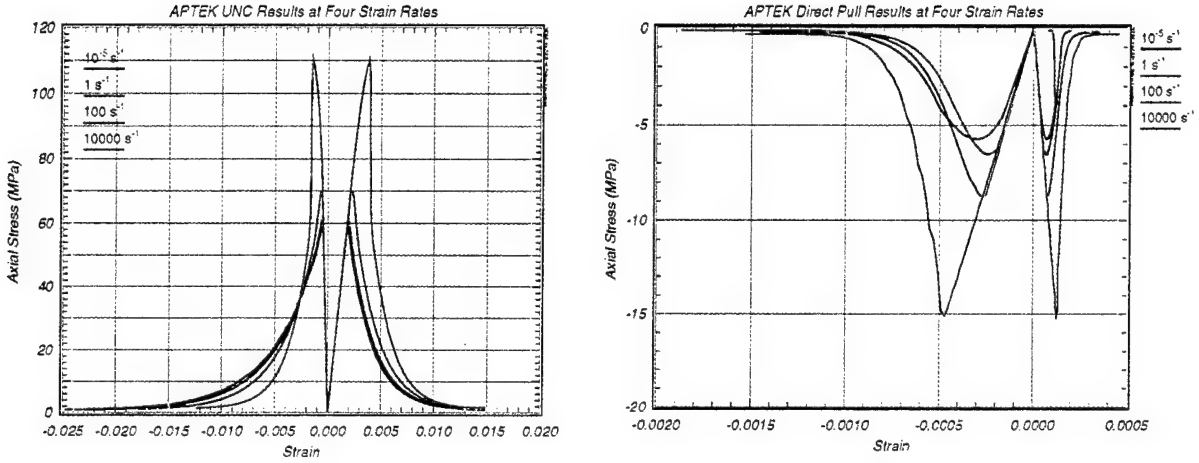


(a) Unconfined compression.

(b) Unconfined tension.

Figure A-5. Uniaxial stress behavior of the model at four strain rates.

# APPENDIX B

## ANALYTICAL SOLUTIONS FOR DUVAUT-LION AND PERZYNA MODELS

We use the viscoplastic update scheme suggested by Simo *et. al.* (1988), except we make the effective fluidity parameter, $\eta_n$, a function of strain rate, as follows:

$$\eta_n = \eta_1 \left(\frac{\gamma}{\dot{\epsilon}}\right)^{(n-1)/n} \tag{B.1}$$

$$\alpha = \frac{1}{\Delta t/\eta_n + 1}$$

$$\bar{\sigma}_{ij} = (1-\alpha)\tilde{\sigma}_{ij} + \alpha\tilde{\sigma}_{ij}^{trial} \tag{B.2}$$

$$\begin{array}{lll} \eta_n \to 0 & \bar{\sigma}_{ij} = \tilde{\sigma}_{ij} & \text{Inviscid Solution} \\ \eta_n \to \infty & \bar{\sigma}_{ij} = \tilde{\sigma}_{ij}^{trial} & \text{Elastic Solution} \end{array}$$

Here $\bar{\sigma}_{ij}$ and $\tilde{\sigma}_{ij}$ are the viscid and inviscid stress tensors, respectively, and $\tilde{\sigma}_{ij}^{trial}$ is the elastic trial stress. At each time step, $\tilde{\sigma}_{ij}$ and $\tilde{\sigma}_{ij}^{trial}$ are calculated and saved by the plasticity algorithm. Then we apply Equation B.2 to update the viscous solution. Note that the inviscid and instantaneous elastic solutions are obtained as limiting cases. The single parameter Duvaut-Lions model corresponds to the $n = 1$ solution.

One motive for extending the single-parameter Duvaut-Lion model to two parameters is to provide a more flexibility in fitting high strain rate data. Similarly, Simo *et. al.* (1988) suggest a form for exponential and power law models which are more flexible in fitting data than their basic single parameter model. However, these more elaborate models require the solution of a nonlinear equation at each and every time step of the finite element calculation. The solution of the nonlinear equation provides the interpolation parameter $\alpha$ as an *implicit* function of strain rate. On the other hand, our proposed implementation provides the interpolation parameter $\alpha$ as an *explicit* function of strain rate. Our implementation eliminates the need to solve a nonlinear equation at each time step. This is an advantage when running large calculations where CPU-time is an issue. Hence, a second motive for extending the single-parameter Duvaut-Lion model to two parameters is to develop an efficient run-time model.

Here we've converted the single-parameter Duvaut-Lion model to a two-parameter model. We say two parameters, rather than three parameters, because $\eta_1$ can be regrouped with $\gamma$ to yield one less parameter. The two parameters for fitting Perzyna-type behavior are $n$ and $\gamma$ with $\eta_1 = 1$. The one parameter for fitting Duvaut-Lions type behavior is $\eta_1$ with $n = 1$.

The form of the fluidity parameter in Equation B.1 is based on comparisons between analytical solutions for Duvaut-Lions and Perzyna power law models. A thorough discussion of the derivation is given by Murray and Lindberg (1996). Perzyna-type power law models are

more flexible in fitting data than the Duvaut-Lions model, because they are three-parameter models rather than single parameter models. However, they are not as easy to implement into existing cap models. In fact, the plasticity algorithm must be rewritten to accommodate the viscoplastic implementation. This is a time-consuming and tedious task, and hence was not undertaken. See Perzyna (1971) for a discussion of Perzyna type models.

For a state of uniaxial stress, the analytical Duvaut-Lions and Perzyna solutions provide the peak dynamic strength (viscid stress) as a function of static strength (inviscid stress) and strain rate as follows:

$$\sigma_{viscid} = \sigma_{inviscid} + E\dot{\epsilon}\eta_1 \left(\frac{\gamma}{\dot{\epsilon}}\right)^{(n-1)/n} \tag{B.3}$$

where $E$ is Young's modulus. One can use Equation B.3 to estimate the effective fluidity parameter when fitting high strain rate data. The resulting behavior in Figure B-1. Here we've plotted the viscid/inviscid stress ratio as a function of $\dot{\epsilon}/\gamma$ for three values of $n$. The $n = 1$ solution provides the largest increase in strength over the smallest range in strain rate: it is the 'steepest' solution.

These numerical peak stress solutions may be fit to Hopkinson bar data by overlaying the solutions onto data plots and shifting right or left until one of the numerical solutions fits the data, as previously demonstrated for Solenhofen limestone data (Green, 1969) in Figure 1-12. The value of $n$ is obtained from the chosen numerical solution and the value of $\gamma$ (Perzyna Parameter) is obtained by equating the overlay abscissa ($\dot{\epsilon}/\gamma$) to the data abscissa ($\dot{\epsilon}$). As previously shown in Figure 1-12, the $n = 1$ Duvaut-Lions solution provides the best fit to the limestone data, although the lone data point at $\dot{\epsilon} = 0.1$ s$^{-1}$ is not fit well. However, the $n = 5$ solution provides a better fit to the concrete data than the $n = 1$ solution previously shown in Figure 1-13. This good fit was previously shown in Figure 1-17. Our two-parameter formulation provides Perzyna-like flexibility in fitting data with the ease of implementation of a Duvaut-Lions model.

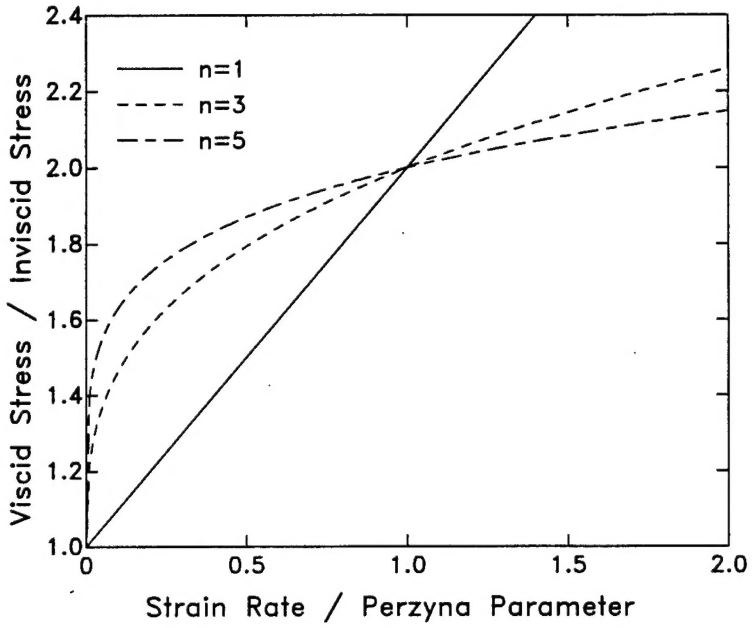


(a) Linear abscissa.

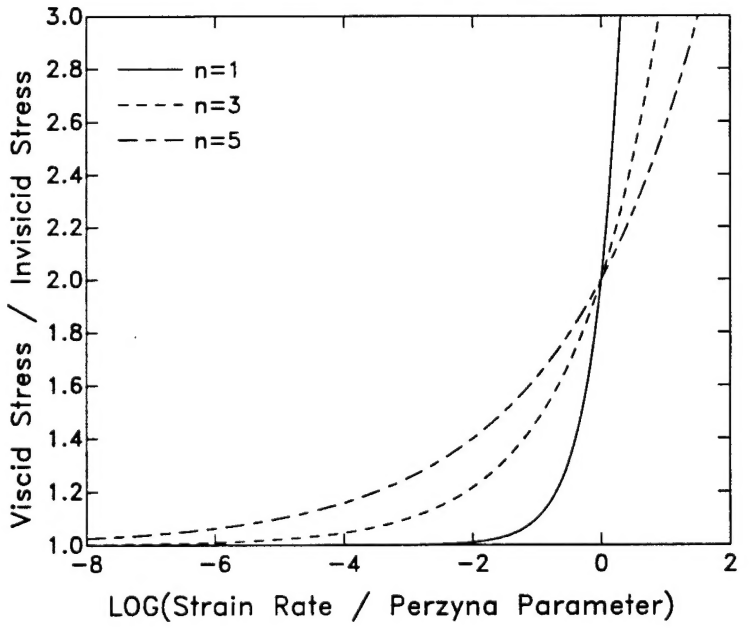


(b) Logarithmic abscissa.

Figure B-1. Numerically calculated strength enhancement indicating that the $n = 1$ solution has the steepest slope.

# DISTRIBUTION LIST

**DSWA-TR-96-16**

**DEPARTMENT OF DEFENSE**

DEFENSE INTELLIGENCE AGENCY
ATTN: DIW-4

DEFENSE SPECIAL WEAPONS AGENCY
2 CY ATTN: ISST
ATTN: OPS
ATTN: P SENSENY
ATTN: D RICE
ATTN: W ULLRICH

DEFENSE TECHNICAL INFORMATION CENTER
2 CY ATTN: DTIC/OCP

FIELD COMMAND DEFENSE SPECIAL WEAPONS AGENCY
ATTN: FCTO
ATTN: FCTOS
ATTN: DR BALADI

**DEPARTMENT OF THE ARMY**

ADVANCED RESEARCH PROJECT AGENCY
ATTN: DEFENSE SCIENCES OFFICE

U S ARMY CORPS OF ENGINEERS
ATTN: CERD-L

U S ARMY ENGINEER DIST OMAHA
ATTN: H GAUBE

U S ARMY ENGR WATERWAYS EXPER STATION
ATTN: C D NORMAN
ATTN: CEWES-SD
ATTN: L K DAVIS
ATTN: DR D BANKS
ATTN: J WARRINER
ATTN: TECHNICAL LIBRARY
ATTN: W MCMAHON
ATTN: W MILLER

**DEPARTMENT OF THE AIR FORCE**

AIR FORCE CTR FOR STUDIES & ANALYSIS
ATTN: AFSAA/SAI

AIR UNIVERSITY LIBRARY
ATTN: AUL-LSE

**DEPARTMENT OF ENERGY**

LOS ALAMOS NATIONAL LABORATORY
ATTN: REPORT LIBRARY

SANDIA NATIONAL LABORATORIES
ATTN: A F FOSSUM
ATTN: J D ROGERS
ATTN: T BERGSTRESSER
ATTN: TECH LIB

**OTHER GOVERNMENT**

CENTRAL INTELLIGENCE AGENCY
ATTN: OSWR/NED

**DEPARTMENT OF DEFENSE CONTRACTORS**

ANALYTIC SERVICES INC (ANSER)
ATTN: K BAKER

APPLIED RESEARCH ASSOCIATES INC
ATTN: C J HIGGINS

APPLIED RESEARCH ASSOCIATES INC
ATTN: S BLOUIN

APPLIED RESEARCH ASSOCIATES INC
ATTN: R FRANK

APTEK INC
ATTN: B LEWIS
2 CY ATTN: Y MURRAY

BOEING TECHNICAL & MANAGEMENT SVCS INC
ATTN: W M LEAVENS
ATTN: A W SPENCER
ATTN: R BRYAN CAIRNS

IIT RESEARCH INSTITUTE
ATTN: DOCUMENTS LIBRARY
ATTN: M JOHNSON

INSTITUTE FOR DEFENSE ANALYSES
ATTN: CLASSIFIED LIBRARY

JAYCOR
ATTN: CYRUS P KNOWLES

KAMAN SCIENCES CORP
ATTN: RICHARD KEEFFE

KAMAN SCIENCES CORPORATION
ATTN: DASIAC

LACHEL AND ASSOCIATES INC
ATTN: C LINAMEN
ATTN: J BECK

LOGICON R AND D ASSOCIATES
ATTN: DR T A PUCIK
ATTN: LIBRARY

LOGICON R AND D ASSOCIATES
ATTN: E HUMPHREYS

MAXWELL LABORATORIES INC
ATTN: K D PYATT JR

NTS ENGINEERING
ATTN: S SHORT

PACIFIC-SIERRA RESEARCH CORP
ATTN: H BRODE

PACIFIC-SIERRA RESEARCH CORP
ATTN: D GORMLEY

SCIENCE APPLICATIONS INTL CORP
ATTN: H PRATT
ATTN: TECHNICAL REPORT SYSTEM

SCIENCE APPLICATIONS INTL CORP
ATTN: W LAYSON

SOUTHWEST RESEARCH INSTITUTE
ATTN: B THACKER

SRI INTERNATIONAL
ATTN: DR JIM GRAN

THE AEROSPACE CORP
ATTN: LIBRARY ACQUISITION

TITAN CORPORATION
ATTN: J THOMSEN

TITAN CORPORATION (THE)
ATTN: LIBRARY
ATTN: S SCHUSTER
ATTN: Y M ITO

TRW SPACE & DEFENSE SECTOR SPACE &
ATTN: W WAMPLER

UTD INC
ATTN: E FOSTER

WEIDLINGER ASSOC INC
ATTN: E WONG
ATTN: H LEVINE

WEIDLINGER ASSOCIATES INC
ATTN: I SANDLER
ATTN: M BARON